IOS

DEACON LABORATORY

RADIOACTIVE WASTE DISPOSAL STUDIES
GEOCHEMICAL ASPECTS OF SITE CHARACTERISATION
FINAL REPORT

BY

J. THOMSON, T.R.S. WILSON, S. COLLEY,

N.C. HIGGS AND D.J. HYDES

REPORT NO. 249

1987

OCEAN DISPOSAL OF HIGH LEVEL RADIOACTIVE WASTE

A RESEARCH REPORT PREPARED FOR

THE DEPARTMENT OF THE ENVIRONMENT

Natural Environment Research Council

INSTITUTE OF OCEANOGRAPHIC SCIENCES DEACON LABORATORY

INSTITUTE OF OCEANOGRAPHIC SCIENCES

DEACON LABORATORY

Wormley, Godalming,
Surrey, GU8 5UB, U.K.

Telephone: 0428 79 4141
Telex: 858833 OCEANS G
Telefax: 0428 79 3066

Natural Environment Research Council

INSTITUTE OF OCEANOGRAPHIC SCIENCES

DEACON LABORATORY

REPORT No. 249

Radioactive waste disposal studies geochemical aspects of site characterisation Final Report

J. Thomson, T.R.S. Wilson, S. Colley,
N.C. Higgs and D.J. Hydes

1987

DOCUMENT DATA SHEET

AUTHOR	THOMSON, J., WILSON, T.R.S., COLLEY, S., HIGGS, N.C. & HYDES, D.J.	*PUBLICATION DATE* 1987
TITLE	Radioactive waste disposal studies: geochemical aspects of site characterisation. Final Report.	
REFERENCE	Institute of Oceanographic Sciences Deacon Laboratory, Report, No.249, 76pp.	

ABSTRACT

This report summarises geochemical research carried out by the Institute of Oceanographic Sciences in connection with the DoE Radioactive Waste Management Research Programme. It covers the period 1 April 1979 to 31 March 1987. Particular attention has been given to the Great Meteor East area of the Madeira Abyssal Plain, and to those natural geochemical species which show mobility in the sediment column.

Much of the work mentioned here is reported upon, usually in much greater detail, in a series of individual reports.

ISSUING ORGANISATION

Institute of Oceonographic Sciences
Deacon Laboratory
Wormley, Godalming
Surrey GU8 5UB. UK.

TELEPHONE 0428 79 4141

TELEX 858833 OCEANS G

TELEFAX 0428 79 3066

KEYWORDS

CHEMICAL OCEANOGRAPHY
GEOCHEMISTRY
RADIOACTIVE WASTE DISPOSAL
RADIONUCLIDE MIGRATION
GREAT METEOR EAST
MADEIRA ABYSSAL PALIN

CONTRACT PECD7/9/308

PROJECT CO 23/33/43

PRICE £21.00

Copies of this report are available from:
The Library, Institute of Oceanographic Sciences Deacon Laboratory.

CONTENTS

1. INTRODUCTION

This report discusses work for the DoE high-level radioactive waste research programme performed by the IOS Marine Chemistry Group in the period 1 April 1979-31 March 1987. An earlier interim report (Booty, 1985) deals with studies carried out between 1979 and 1984. The present report is concerned mainly with the area of the Madeira Abyssal Plain termed Great Meteor East (GME) which has been studied by scientists of several countries in a programme co-ordinated by the OECD Nuclear Energy Agency's Seabed Working Group. A certain amount of work from other areas identified earlier by the Seabed Working Group was also undertaken and is reported herein (Sections 8 & 9 and Appendices 1, 2, 8 & 10).

The GME area is not strictly defined but is broadly the area bounded by 30-33°N and 23-26°W. A reconnaissance visit was made in 1982 (RRS Discovery Cruise 129) and the site was worked intensively by the IOS Marine Chemistry Group in 1984 (RRS Discovery Cruise 149). Three members of the Group also participated in the 1985 cruise of the French vessel Marion Dufresne to the area. A further cruise took place later in the contract (RRS Discovery Cruise 160 in 1986) mainly directed towards the gathering of geochemical information in the 10 x 10 km box in GME selected by the DoE early in 1985 for intensive study.

Seabed sediments consist of two components, the solid phase, which is composed of mineral and biogenic particles ranging from colloidal size up to several hundred micrometres, and the solution phase (pore water) which is originally derived from buried sea water and occupies the intergranular space. In the pore water, dissolved material can move slowly through the sediment, either by bulk movement of the pore water (advection), or by random movement at the molecular level (diffusion). The solid phase surfaces are, however, not inert; they can attract and adsorb dissolved material by a variety of mechanisms. If a given dissolved ion or molecule is strongly adsorbed, it will spend most of the available time on sediment particle surfaces, and very little time actually in solution. Consequently, movement by diffusion or advection will be inhibited strongly by the adsorptive mechanism. To predict the movement of a waste radionuclide within deep-ocean sediment, it is necessary to establish how strongly the radionuclide is adsorbed on the sediment. The physico-chemical nature of the total sedimentary environment must be determined as well as the nature of the solid phase material. The valence state of many radiologically-important radionuclides depends on the environmental redox

potential. In turn, the degree to which such radionuclides bind to the surface of sediment particles changes with their valence state. Hence, the rate at which a particular radionuclide will migrate through the sediment, either by diffusion or by pore water movement, is controlled by the environmental redox potential. Practically, the environmental redox state can only be investigated by pore water studies.

Other factors may also exert an influence; in particular, a radionuclide may form complex ions or molecules by association with one or more of the chemical species present in the pore water. Such complexation may be very significant in modifying the behaviour of a radionuclide, and it is important to identify precisely which chemical forms of the element of concern are likely to be present.

It follows from the foregoing that the objectives of the present study require that the solid and solution phase compositions should be well characterised, that the processes which determine the physico-chemical state of the system should be understood, and that the stability of such systems over time should be assessed. Sections 3 to 8 of this report summarise the progress which has been made towards these goals; Section 11 concerns work which remains to be done before a complete and informed assessment of the proposal can be undertaken. It is particularly important to note that the present study was concerned with the properties of the natural, undisturbed system, and is therefore relevant to the waste 'far field'. Because of this, particular emphasis has been placed on the geochemistry of elements which are mobile under natural conditions.

The stability of the sedimentary system towards the disturbance caused by the emplacement and presence of waste containers has been addressed only indirectly, since the 'near field' composition and corrosion behaviour of the waste have not yet been defined.

2. MADEIRA ABYSSAL PLAIN: DEPOSITIONAL ENVIRONMENT

Deep ocean sediment forms continuously by the slow deposition of particles of mainly mineral and biological origin. This process (pelagic deposition) produces sedimentation rates typically of the order of 1 cm per thousand years. Occasionally, sediment accumulated on a continental shelf and slope, or on a seamount, may become unstable. This may occur as the result of a tectonic or other disturbance, and slumping towards deeper water can then produce a 'turbidity flow', which consists of a relatively high-density mobile slurry. Initially these flows may be quite restricted laterally, and may indeed follow defined channels at surprisingly high velocities. Later, as the seabed slope declines, the flow typically slows and spreads over a wider area, and the coarser material settles out. The beds of sediment emplaced rapidly by this process are known as 'turbidites'. Near to the source zone, turbidites frequently show a striking vertical gradient in grain size due to differential sedimentation. At the greatest distance from the source zone, only the finer particles remain in suspension. Consequently, distal turbidites are relatively fine-grained and homogeneous.

Piston cores taken on the GME abyssal plain reveal that distal turbidite units form the major part of the sedimentary succession. These cores contrast markedly with the entirely pelagic sediments observed on the small topographic highs in the same area. Between the turbidites on the plain, thin units of the same pelagic sediments are found which may be correlated and dated by means of their coccolith distributions (Weaver & Kuijpers, 1983; Searle *et al.*, 1985; Weaver & Rothwell, 1987). Individual turbidites can be correlated over a wide area, although their individual thicknesses vary over the area of the plain dependent on the direction of the emplacement flow of the particular turbidite. The large number of GME piston cores collected by IOS and Dutch scientists has allowed establishment of an excellent stratigraphy to depths of 10-15 m. Because piston cores often have a poor recovery of the uppermost sediments, however, the distribution and thicknesses of the most recent turbidites (*a* and *a1*, emplaced about 200 and 10,000 years ago, respectively) are less well defined. The box cores collected by the IOS Chemistry Group provide some delineation of the surface sediments: generally turbidite *a* is thickest (> 0.5 m) to the west of the area and thins to the east, while turbidite *a1* is generally < 1 m thick and thins east to west. The study of these two recent turbidites is important to understand the post-depositional geochemical redistributions which are recorded in most of the deeper turbidites. Only in

the active surface examples can the pore water environment be investigated to elucidate the geochemical processes responsible for element redistribution.

The major reductants found in deep sea sediments are compounds of organic carbon. In a slowly accumulated (pelagic) sediment, the flux of carbon sedimented is oxidised at the sediment/water interface so that only traces of refractory organic carbon (~ 0.3%) are accumulated and buried. Such sediments are termed oxic because free oxygen remains in pore water solution to considerable depth, perhaps tens of metres. The sediment which gave rise to the GME turbidites were accumulated more rapidly than this, and consequently have a higher organic carbon content. The presence of large thicknesses of turbidites with enhanced levels of organic carbon has important consequences for the redox status of the GME sediments, as will be discussed.

Redox considerations are important because this study has placed particular emphasis on those elements which migrate within the sediments. This class includes Mn and Fe, both of which respond to the redox status of the sediments and also form oxyhydroxides of considerable sorptive capacity. The GME turbidites are, for the most part, fine-grained and structureless, with occasional silt laminae at their bases (Weaver & Kuijpers, 1983). As a consequence, the turbidites have remarkably consistent inert element compositions in the vertical against which redox-sensitive element profiles may be contrasted. This facilitates the geochemical interpretation of solid-phase data.

3. PORE WATER STUDIES

The pore waters of marine sediments are in intimate contact with the solid phase. In deep-ocean sediments, this phase is usually fine-grained so that the movement of the pore water relative to the solid phase, if it occurs at all, is very slow. Reactions with the solid phase alter pore water composition. The pore water at shallow depths is still in communication with the overlying sea water by the process of molecular diffusion, however, which tends to restore the pore water composition to that of sea water. This transport process is slow and, even close to the sediment-water interface, quite large changes in pore water composition occur (Figs. 3.1 & 3.6). Study of these pore water composition changes can reveal important information about the interactions between the solid and solution phases. Since mineralogical and chemical changes in the solid phase are often difficult to quantify, study of the pore water composition can provide useful information not otherwise available.

The simplest practical method of obtaining pore water for analysis is to squeeze or centrifuge it from core samples. Unfortunately, pore water composition can be altered during recovery by effects related to pressure and temperature changes and by contamination and oxidation. Stringent precautions, such as processing of core samples at in-situ temperatures in a nitrogen-filled glove box, can ameliorate these effects; but sampling of pore waters by filtration on the sea bed is also necessary to validate the shipboard procedures and to correct for pressure effects. This requires specially developed sea-bed instrumentation. The value of in-situ sampling instruments was illustrated during the present study when it was found that pore water uranium values obtained by other means are not reliable because of pressure effects (Appendix 3).

Early in our studies of the GME site, it became clear that the turbidite depositional pattern imposed a redox behaviour quite distinct from that observed in ordinary pelagic environments. This point is best illustrated by a consideration of Figure 3.1, which is a composite of data obtained at two stations from corer and in-situ device samples. Figure 3.1 shows that the pore waters at Station 10552 (a normal pelagic station) are well oxygenated; there is no evidence of nitrate consumption, and dissolved manganese remains below detection limits at all depths. Station 10554, at the GME site, shows a more complex and active character. Pore water oxygen levels fall off rapidly with depth and reach zero close to the surface of a conspicuous green layer, shown in Figure 3.2. Nitrate levels also decrease continually from a near-surface

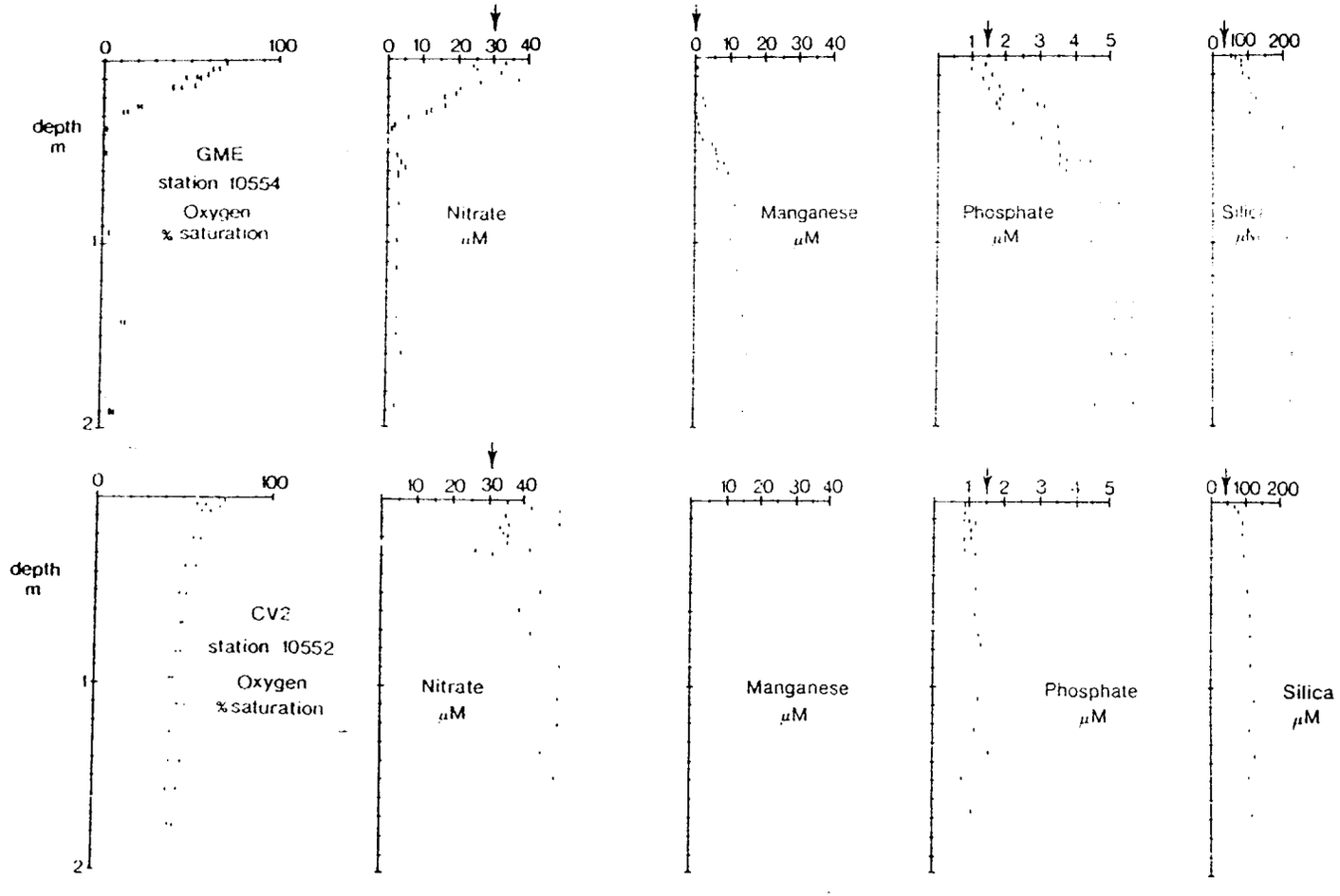

Porewater data; comparison of stations 10552 and 10554. This figure is a composite of data from both cores and porewater samples. No manganese in solution was detected at station 10552.

Fig-3-1

maximum and fall to zero at a depth only slightly greater than that for oxygen. Traces of nitrate and of oxygen are observed below the green layer. It is noteworthy that the depth profiles for both oxygen and nitrate above the green layer are linear. Manganese is found in solution at depths below the top of the green layer but does not co-exist in solution with appreciable quantities of oxygen.

The key to understanding these pore water profiles lies in the nature of the sediments and their accumulation at the two sites. At Station 10552 the thorium-230 data (Fig. 3.3) shows an unusually deep, near-surface mixed layer underlain by a zone of regular decrease from which a mean sediment accumulation rate of 0.42 cm kyr^{-1} may be estimated. This compares with estimates of 0.32 cm kyr^{-1} and 0.41 cm kyr^{-1} obtained from the palaeontological evidence shown in Figure 3.3. These low values indicate that this is a pelagic sediment, although accumulation may have been somewhat irregular with time. The bulk accumulation rate is well below the value of 4 cm kyr^{-1} suggested by Müller and Mangini (1980) as being required for the development of anoxic conditions. It appears that, as they predict for this situation, all labile organic carbon is degraded close to the sediment-water interface so that the pore water profiles are those of a well-oxygenated sediment at steady state (Froelich et al., 1979). Under such conditions little migration of redox-sensitive elements will occur. The SiO_2 and Al_2O_3 profiles, taken as indicators of the detrital or clay component of the sediment, have a shape the mirror-image of that of carbonate. When this carbonate dilution effect is removed by expression on a carbonate-free basis, the MnO profile approximates to a constant value. This contrasts with Station 10554 (Fig. 3.5) where mobilisation at depth under reducing conditions permits migration into the upper oxic layer and fixation as a diagenetic near-surface enrichment of manganese.

The area in which Station 10554 is located has been studied by Weaver and Kuijpers (1983) who demonstrated that pelagic sediment accumulation is interrupted sporadically by thick turbidite units which possibly arise on the NW African margin. Over the past 3×10^5 years the pelagic accumulation rate has averaged 0.5 cm kyr^{-1}, while the overall accumulation rate is 10 cm kyr^{-1} because of the turbiditic contribution (P.P.E. Weaver, personal communication). It is important to note that these are extreme distal turbidites, showing little evidence of size grading even in examples some metres thick. Many of the turbidites have relatively high (> 1%) organic-carbon contents. The green layer mentioned above has an organic carbon content of 1.6% and exhibits sharp

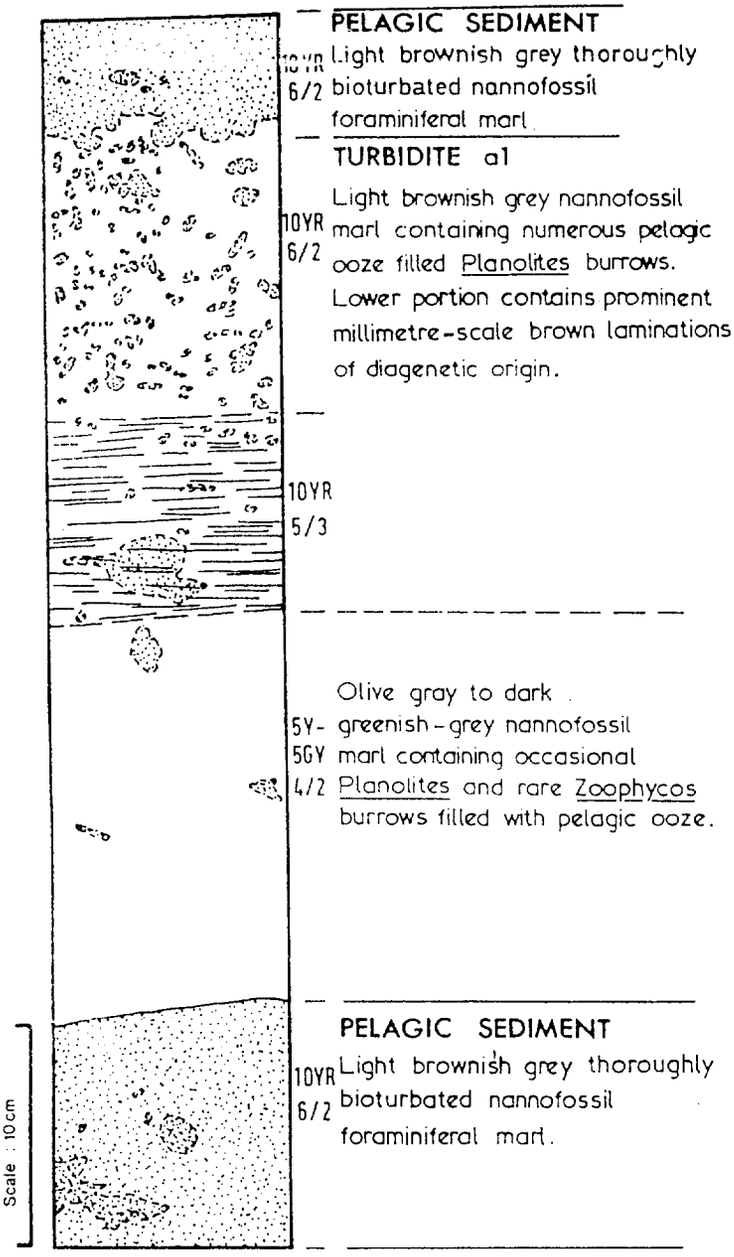

Cross-section of boxcore subcore taken at station 10554 showing main lithological units discussed in the text.

Fig. 3.2

contrasts, top and bottom. However, the compositional data, palaeontological observations and thorium-230 data lead to the important conclusion that the green layer is, in fact, only the lower part of a larger turbidite unit. Figure 3.5 shows the depth profiles of thorium-230, SiO_2, CaO and Al_2O_3 in a box core from Station 10554. (Total thorium-230 is plotted here rather than thorium-230-excess because of the mobility of uranium at this site, a feature further discussed in Section 6). The top 0.6 m of the core is entirely Holocene, on the evidence that the coccolith Emiliana huxleyii is the dominant species. There are no foraminifera present in the turbidite, apart from those in burrows worked down from the surface pelagic sediment to the upper part of the turbidite. The turbidite therefore lacks the coarser-grained fraction which typifies the pelagic carbonates of the area. The thorium-230 (total) data indicate a high surface value, as would be expected from pelagic accumulation, but the downward mixing by bioturbation occurs over 15 cm or so to a lower value of 6-7 dpm g^{-1} which characterises the turbidite. Below the sharp base of the green layer, a high thorium-230 (total) value of 18.5 dpm g^{-1} is found, again indicating sediment formed under pelagic conditions. The SiO_2, Al_2O_3 and CaO profiles are consistent with this interpretation. Because of bioturbation, the depth of the top of the turbidite cannot be defined precisely but the section from 12 cm to the base at 51 cm appears largely homogeneous.

What then is responsible for the difference in appearance of the upper (brown) zone and the lower (green) zone of the turbidite? Considering the oxygen and nitrate pore water profiles (Fig. 3.1), their relationship to the onset of the green colouration, and the solid-phase organic carbon profile (Fig. 3.4), it is inferred that the colour change represents a downward-moving oxidation front. The rate of movement of this front is controlled, inter alia, by the rate of diffusion of oxygen and nitrate from the bottom water to the front. Thus, the brown upper section is the part of the turbidite where reactive organic carbon has been metabolised and which is now oxic. The linear profiles of oxygen and nitrate indicate that oxidation occurs at a restricted locus of activity, at or near the colour change boundary, rather than throughout the sediment thickness above this layer. Initially, it was considered that the colour change might be related directly to the step in organic-carbon content which occurs at the colour change boundary, but the recent paper by Lyle (1983) demonstrates that such colour changes are often related to redox changes in the lattice iron content of clay minerals. Experimentally, the colour of both parts of the turbidite may be changed reversibly by treatment with oxidising or

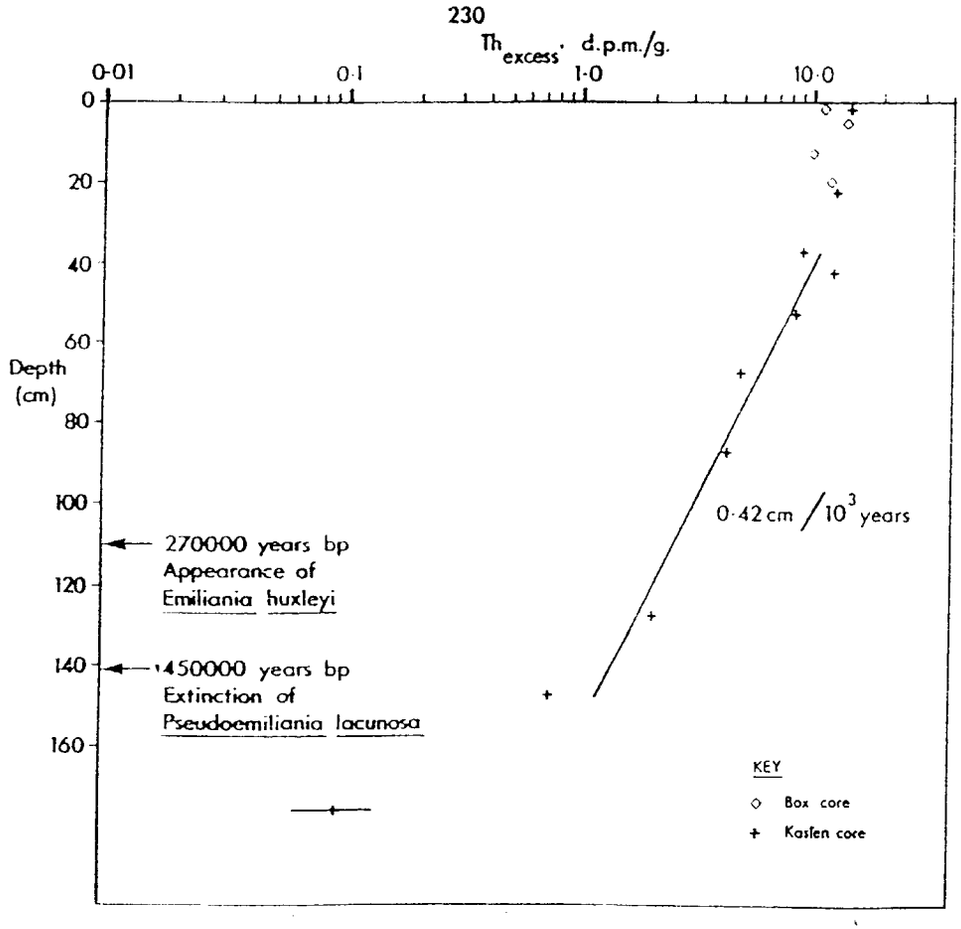

Composite profile of $^{230}Th_{excess}$ activity *versus* depth for two cores at station 10552. The accumulation rate estimate is calculated from the slope of the regression line shown. Coccolith data obtained from P. P. E. Weaver.

Fig. 3. 3

reducing agents. This observation indicates that, although organic-carbon content may influence sediment colour, the redox profile exerts the major influence on the colour of the sediment through the direct mechanism described by Lyle (1983). Further evidence of a strong redox gradient in the colour-change region of the core is provided in Figure 3.4. The step in solid-phase manganese concentration which occurs in the brown zone above the colour interface is caused by migration of manganese in the pore waters from below and precipitation at this point on the rising redox gradient. The pore water manganese profile (Fig. 3.4) shows that manganese is being supplied to the bottom of the solid phase peak in this manner. A peak in the uranium concentration also occurs in the green band, about 2 cm below the colour change. A similar observation had previously been made in a core from the Cape Verde Abyssal Plain (Appendix 1). As here, the peak was attributed to a post-depositional mobilisation of uranium originally associated with organic matter in response to the progess of an oxidation front; preferential downward migration is caused by fixation deeper in the sediment under reducing conditions. A third redox-related feature is the slight decrease in CaO of the brown section of the turbidite relative to the green section. This is believed to be due to carbonate dissolution consequent on the production of CO_2 when organic carbon is oxidised.

The concept of a progressive downward migration of an oxidation front into a turbidite is not steady-state but implies a continuing readjustment of the redox profile after the emplacement of organic-rich sediment. Initially, this turbidite sediment is present at the sediment-water interface and oxygen from bottom water rapidly raises the redox potential of the uppermost centimetres. This higher redox potential front thus moves downwards as reaction proceeds. This is in contrast to the steady-state behaviour, customarily assumed in deep-sea sediments, in which subsurface redox boundaries track upwards to maintain a constant separation from the sediment-water interface. On this interpretation, it would be predicted that organic-rich turbidites which are exposed under pelagic conditions at the ocean floor for any length of time subsequent to deposition should exhibit organic-carbon removal in their uppermost section due to oxidation. Examination of piston cores taken in the Madeira Abyssal Plain region confirms that this diagenetic phenomenon is commonly found in the upper layers of organic-rich distal turbidites, and it may be inferred from this that the behaviour described has been a recurrent feature in this area for at least 3×10^5 years (Weaver & Kuijpers, 1983).

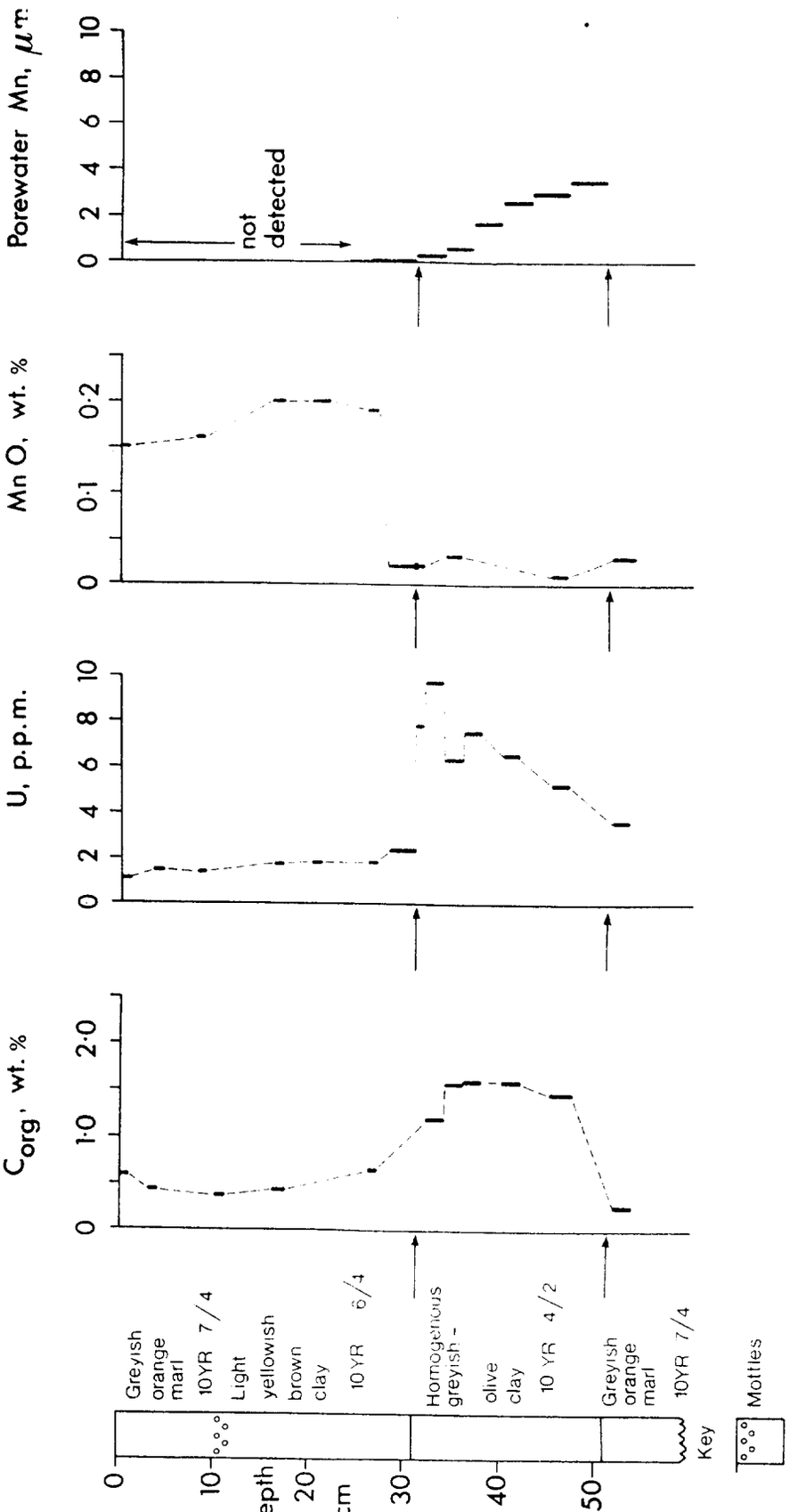
C_{org}, wt. %
0
1·0
2·0
U, p.p.m.
0
2
4
6
8
10
Mn O, wt. %
0
0·1
0·2
Porewater Mn, μm
0
2
4
6
8
10
not detected
Depth cm
0
10
20
30
40
50
Greyish orange marl 10YR 7/4
Light yellowish brown clay 10 YR 6/4
Homogeneous greyish - olive clay 10 YR 4/2
Greyish orange marl 10YR 7/4
Key
Mottles

Fig - 3 - 4

The idea that an oxidation front can progressively 'burn down' into an organic-rich layer potentially has wide applicability. In pelagic conditions, any site which has an organic-rich layer at shallow depth is likely to exhibit this type of secondary subsurface maximum in metabolic activity. The consequences of such behaviour are difficult to predict without a quantitative treatment. One approach is to model the progress of a diagenetic oxidation front into an organic-rich layer by a time-stepped numerical model. The rate of reaction may be computed from the diffusion-limited supply of electron-acceptors. A new diffusion depth is then calculated and is used to recalculate the diffusion gradient, and hence the flux, applicable to the next time-step. The development of this model is described in detail in Appendices 1, 4 and 5. The model predicts the rate of migration of the subsurface oxidation front downwards as the solid-phase organic carbon is oxidised. The treatment for turbidite a1, described in Appendix 4, shows that the total metabolic activity in this turbidite is very similar to the activity at a pelagic station of similar depth. This illustrates the important point that the distribution of metabolic activity exerts a very significant influence; at the pelagic station, all the activity is concentrated at the sediment-water interface in the presence of abundant oxygen. Consequently, the sediment remains oxic. At the GME site, the presence of a significant fraction of the total metabolic activity at the oxidation front within the sediment leads to a total depletion of pore water oxygen and a markedly more reduced sediment profile. In Section 6 it is shown that the migration speed of uranium within the sediment system is profoundly influenced by the oxidation front phenomenon, being much lower in the suboxic GME sediments than in those containing dissolved oxygen. The more recent turbidite a, although basically very similar, is more complex to model. Because of the lower organic carbon content of this sediment, the upward diffusional fluxes of iron and manganese are relatively more important and cannot be ignored. When these are taken into account (Appendix 5), a time of about 200 years since the emplacement of turbidite a is derived.

This date is in broad agreement with those found independently using biostratigraphical and radiological techniques, although it must be emphasised that the present uncertainties in this approach imply an accuracy of no better than a factor of two in this estimate.

Previously published treatments, which model deep-ocean sedimentation as a steady-state process, do not fit the GME observations. In particular, they do

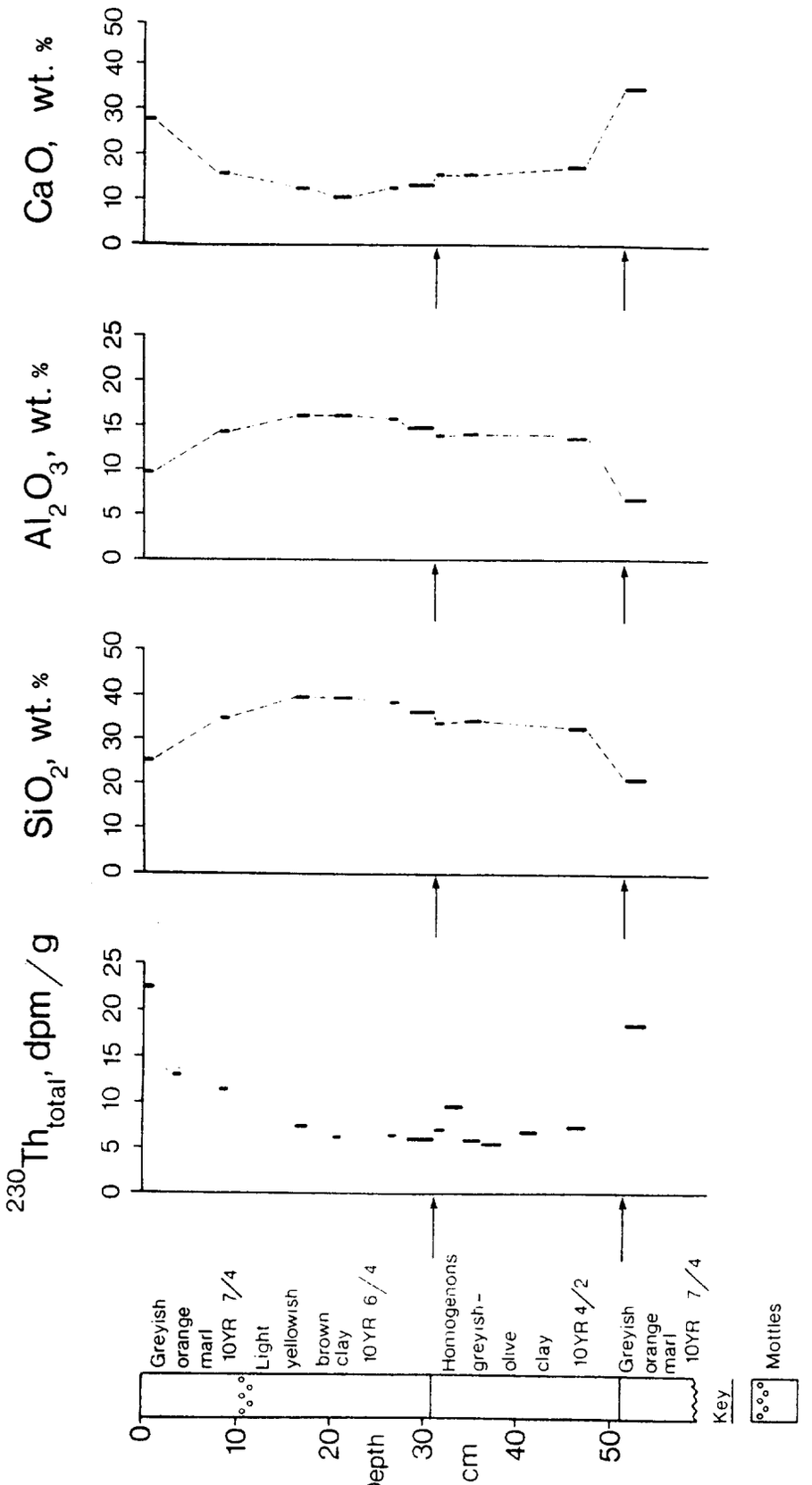
$^{230}Th_{total}$, dpm/g
SiO_2, wt. %
Al_2O_3, wt. %
CaO, wt. %
0 5 10 15 20 25
0 10 20 30 40 50
0 5 10 15 20 25
0 10 20 30 40 50
Depth cm
0
10
20
30
40
50
Greyish orange marl 10YR 7/4
Light yellowish brown clay 10YR 6/4
Homogenous greyish-olive clay 10YR 4/2
Greyish orange marl 10YR 7/4
Key
Mottles

Fig-3-5

not predict the suboxic (mildly reducing) conditions actually observed. By contrast, the oxidation front mechanism fits the observations well. The development of this fundamentally different non-steady state concept (Appendices 1, 4 & 5) underpins our interpretation of the GME dataset.

The pore water data considered thus far were collected on the 1982 and 1984 cruises of RRS Discovery. The IOS results from the 1985 ESOPE exercise are primarily concerned with solid phase uranium data (Appendix 14), but the pore water data collected on this cruise support the oxidation front hypothesis and show that the suboxic conditions mentioned above persist to a depth of at least 30 m. This indicates that the oxidation front cycle described in this report has been the dominant redox determinant at this site for at least the last 800,000 years.

The 10 km square area of the GME site designated as the 'intensive study area' was not selected until after the 1984 Discovery cruise. Consequently, the final site visit in 1986 (Cruise 160) was directed at the intensive sampling of this area in order to compare it with the earlier dataset. The resulting data, which have not yet been published, indicate that the intensive area shares the broad geochemical characteristics already described (Fig. 3.6). It is, however, slightly less reducing than the site described in Appendix 4, apparently because the penultimate turbidite (a1) attained only a modest thickness in this region.

At the intensive study site, this turbidite appears to have been completely oxidised some time before the arrival of the last turbidite (a), which occurred well within the last 500 years. Although the arrival of turbidite a sealed off the sediment below from contact with bottom water, this sediment is still detectably more oxidising than the corresponding material from Station 10554. This station, visited in 1982, exhibits the greatest thickness of turbidite (a1) observed during our studies (Appendix 4), and consequently this turbidite was not completely oxidised before burial. Further work is needed on the data to validate this analysis of the observations (Section 11), since the persistence of oxygen and nitrate below turbidites a and a1 seems anomalous. Broadly, however, the data indicate that the intensive study area is similar to all other Madeira Abyssal Plain stations studied in this programme, in that the oxidation front mechanism has been the major determinant of the redox status of the sediment and pore waters. The application of this concept to a study of the migration of natural radionuclides over the past 800,000 years is given in Section 6.

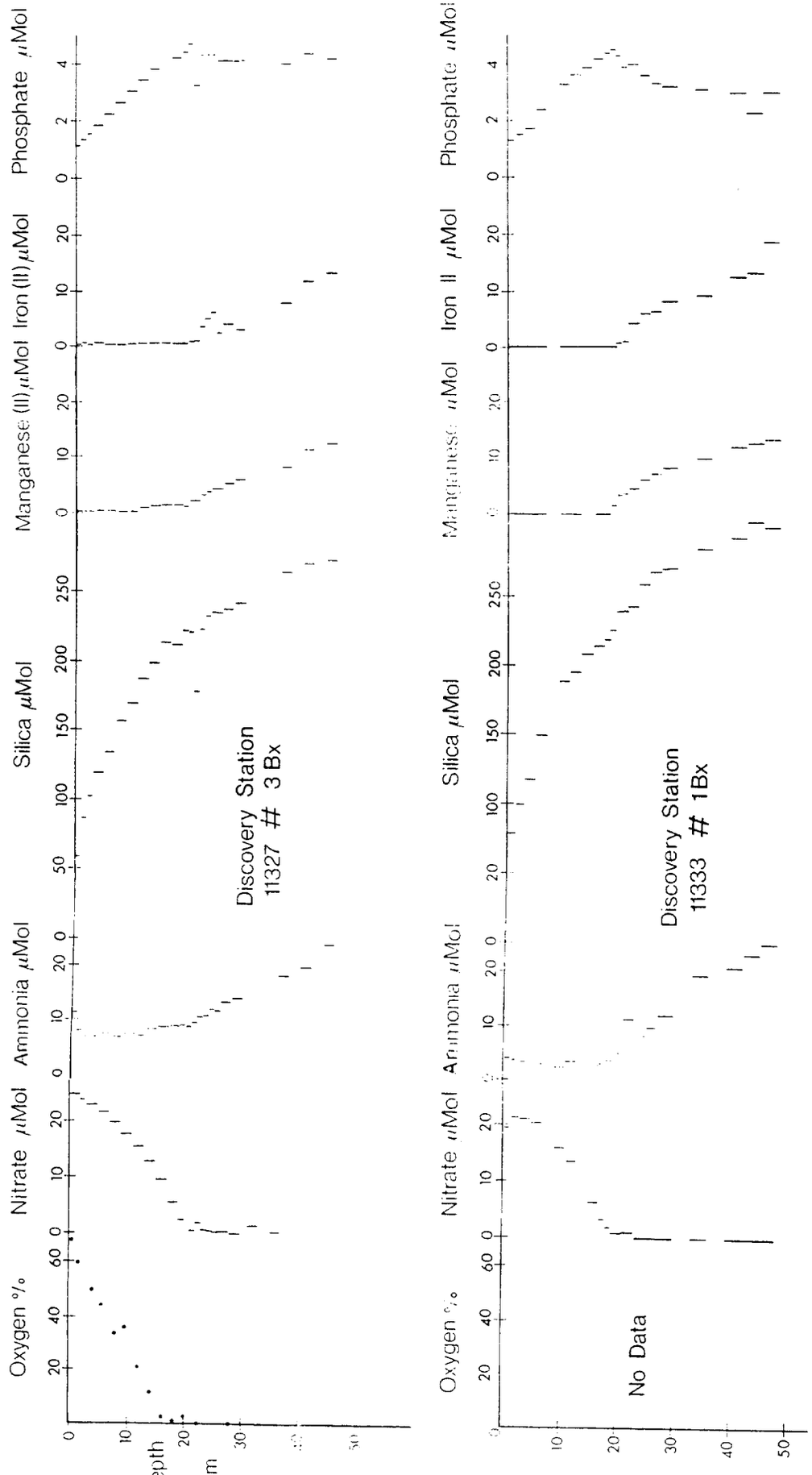
Oxygen %
Nitrate μMol
Ammonia μMol
Silica μMol
Manganese (II) μMol
Iron (II) μMol
Phosphate μMol
Depth cm
Discovery Station
11327 # 3 Bx
Oxygen %
Nitrate μMol
Ammonia μMol
Silica μMol
Manganese μMol
Iron II μMol
Phosphate μMol
No Data
Discovery Station
11333 # 1Bx

Fig-3-6

4. BIOTURBATION IN TURBIDITE a

Bioturbation, the effect of benthic or infaunal organisms in mixing sediments, is an important process in all oxic sediments. Inter alia, it affects the resolution of detail contained in the sedimentary record (e.g. Peng & Broecker, 1984) and in pore water fluxes and signals of chemical diagenesis in the region of the sediment/water interface (e.g. Schink & Guinasso, 1978). In a radioactive waste context, bioturbation will mix radionuclides sorbed at the sediment surface deeper down into the sediments. Few attempts were made to quanitify bioturbation until the last decade (Goldberg & Koide, 1962; Berger & Heath, 1968). During this period, however, many such estimates have been obtained from studies of the near-surface distributions of various natural and fallout radionuclides (Guinasso & Schink, 1975; Nozaki et al., 1977; Turekian et al., 1978; Peng et al., 1979; DeMaster & Cochran, 1982; Aller & DeMaster, 1984; Druffel et al., 1984; Cochran, 1985; Li et al., 1985; Stordal et al., 1985). These deep-sea studies, together with work from other environments, are extensively referenced in a recent review of the mathematical basis of the models used to obtain such estimates (Boudreau, 1986a,b).

The principle behind these methods to estimate bioturbation is that short-lived natural or artificial fallout radionuclides delivered to the sediments from the water column are distributed into the sediments by bioturbation. All studies suggest that deep-sea bioturbation is active over the depth range 5-20 cm downwards from the sediment surface, with an average value of about 8 cm. While the distribution of sediment infaunal biomass suggests that mixing intensity ought to decrease from the surface downwards, most studies have modelled the process with a constant biomixing coefficient D_B. The depth achieved by a particular nuclide is dependent on its half-life as well as the bioturbation coefficient and the mixed layer depth. Deep-sea sediments generally have low accumulation rates so that burial can be ignored. Thus $^{234}Th_{excess}$ ($t_{\frac{1}{2}}$ = 24.1 d) activities fall exponentially over a few cm and are relevant to mixing on a 100-day time scale (Aller & DeMaster, 1984), $^{210}Pb_{excess}$ ($t_{\frac{1}{2}}$ = 22.26 y) activities fall exponentially over several cm and are relevant to a 100-year time scale (Cochran, 1985), and ^{14}C ($t_{\frac{1}{2}}$ = 5730 y) activities are approximately constant over the full depth of the mixed layer because this nuclide largely survives through the mixed layer to be buried below it (Officer, 1982).

The work here was undertaken to ascertain whether bioturbation was similar in the GME area to other deep-sea locations, as has been assumed for modelling

purposes (Appendices 4 and 5). It is not immediately evident that this should be expected: turbidite a was emplaced around 200 years ago (Appendix 5), so that a new sediment surface was formed at that time over the GME plain. The $^{210}Pb_{excess}$ method was selected because it is relevant to mixing on this magnitude of time scale and because more data are available from this method for comparison with other deep-sea deposits from a range of localities. Previous work, however, has been performed on continuously accumulated sediments which may be expected to have had mature benthic and infaunal communities at all times.

Six box cores were selected to represent the GME plain, all with pore water data profiles to confirm good interface recovery. Solid phase data determined by XRF were available from five of the cores for intercomparison. At all six locations turbidite a was the uppermost unit, but only core 11334 fully penetrated the turbidite (Table 4.1). The horizontal and vertical compositional consistency of the turbidite is demonstrated by the similar SiO_2, Al_2O_3 and CaO (mainly from $CaCO_3$) values in the six cores (Table 4.1). The most notable aberrations are the lower CaO and higher SiO_2 and Al_2O_3 values commonly found in surficial samples, and the reverse in the lowest sample of core 11334. The former effect may be due to calcite dissolution at the sediment/water interface because the GME plain is below the calcite lysocline, while the latter is probably a turbidite grading effect. Overall, however, the data attest to a remarkably regular composition in the six cores, which are separated by up to 110 km north/south and 95 km east/west (Fig. 4.1).

^{210}Pb measurements were made by the method of Smith and Hamilton (1984), which employs a leaching procedure and actually measures ^{210}Po as a proxy for ^{210}Pb. The short half-life of ^{210}Po ($t_{\frac{1}{2}}$ = 138.4 d) assures that this is a satisfactory procedure. All data for the six cores are displayed on Figure 4.2, which demonstrates clearly that a rather regular ^{210}Pb activity exists in all cores below 10 cm, while there is a higher value, due to the presence of $^{210}Pb_{excess}$, only above 10 cm. $^{210}Pb_{excess}$ data are obtained either by estimation of a background or support ^{210}Pb level from the gross ^{210}Pb activity/depth profile at depth, or from an independent measurement of the ^{226}Ra parent of ^{210}Pb. The former approach is selected here because of the compositional homogeneity of turbidite a. A support level of 4.4 dpm/g has been calculated (Table 4.2), and the resultant $^{210}Pb_{excess}$ profiles from the cores are presented on Figure 4.3. Values greater than 0.2 dpm/g above this support level have been accepted in the upper 10 cm. Cochran (1985) has

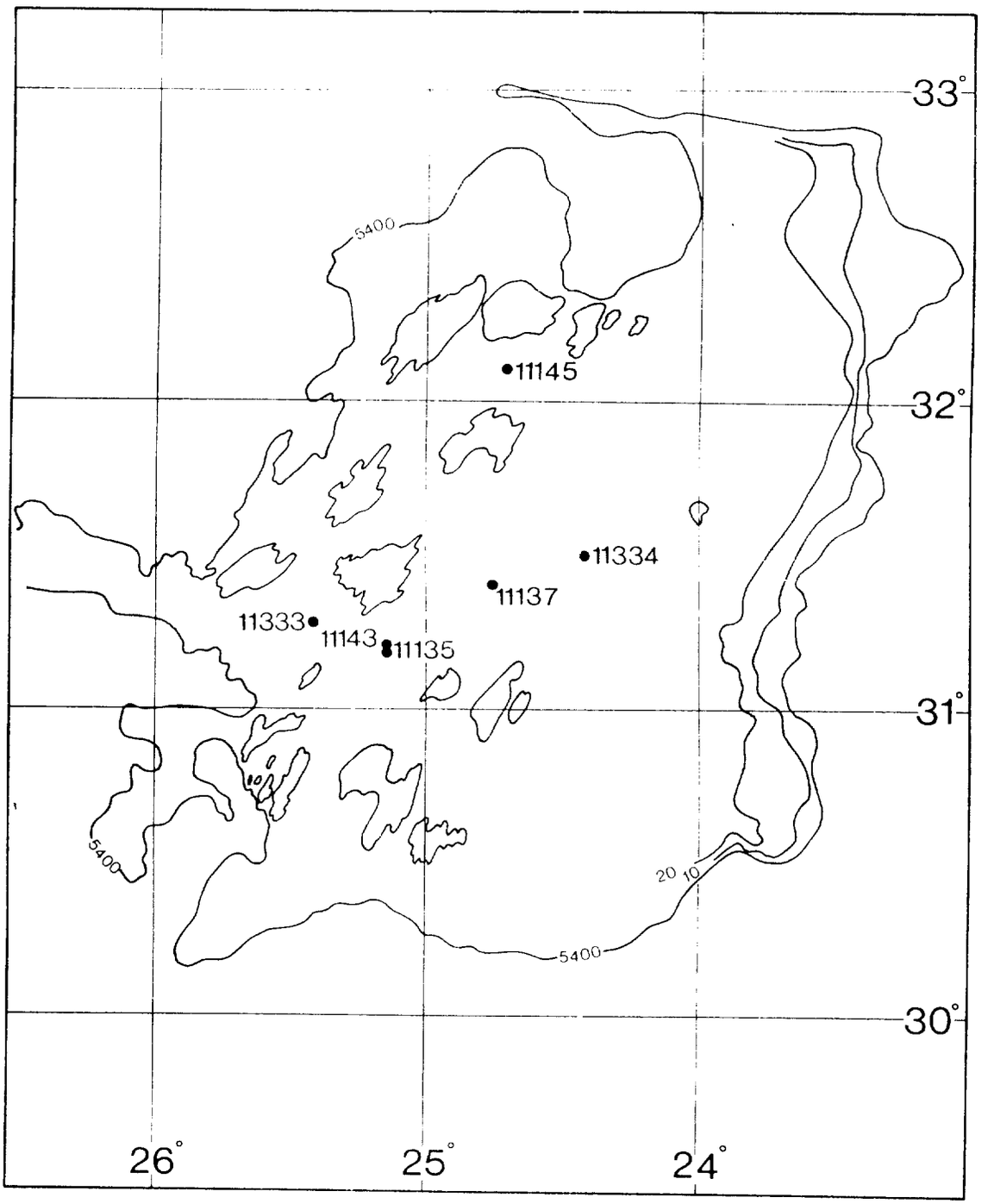

Figure 4.1 Simplified bathymetric map of the GME area showing the locations of box cores used for bioturbation studies.

TABLE 4.1 - Compositional data for the cores sampled

CORE	11135	11137	11145	11333	11334
Length of turbidite a (cm)	> 52	> 58	> 54	> 48	18
No. of samples analysed	15	15	15	20	6
Mean SiO_2 ± 1σ (wt %)	20.29 ± 0.13	20.08 ± 0.36	19.92 ± 0.39	19.80 ± 0.30	20.52 ± 1.06
Range (wt %)	20.06 - 20.55	19.37 - 20.65	19.31 - 20.84*	19.42 - 20.52*	19.49 - 22.34**
Mean Al_2O_3 ± 1σ (wt %)	6.70 ± 0.08	6.72 ± 0.16	6.59 ± 0.22	6.68 ± 0.20	7.44 ± 0.66
Range (wt %)	6.59 - 6.88	6.43 - 7.06	6.32 - 7.21*	6.49 - 7.12*	6.96 - 8.79**
Mean CaO ± 1σ (wt %)	35.19 ± 0.53	34.96 ± 0.51	35.05 ± 0.38	34.89 ± 0.46	33.88 ± 1.07
Range (wt %)	33.47* - 35.78	33.90 - 35.68	34.40* - 35.78	33.36* - 35.42	32.10** - 35.09

* denotes surface (0-1.5 or 0-2 cm) sample, probably affected by calcite dissolution.

** sample at base of turbidite a, core 11334 only. Probable grading effect.

TABLE 4.2 - ^{210}Pb data for all cores

* Mean values quoted are weighted mean and standard deviation for all points from each core except those for which a $^{210}Pb_{excess}$ value is cited.

** Inventory = $\sum_{1}^{n} {}^{210}Pb_{excess}$ x <u>in-situ</u> dry density x sample thickness, for each $^{210}Pb_{excess}$ value in a core. Some samples with an expected $^{210}Pb_{excess}$ value are missing.

Note: The <u>in-situ</u> dry density of these sediments (i.e. dried weight including salt divided by wet volume) is 0.5 g/cm^3.

Core 11135

Depth cm	^{210}Pb dpm/g	$^{210}Pb_{excess}$ dpm/g
0-2	8.2 ± 0.3	3.8 ± 0.3
2-4	4.95 ± 0.15 4.01 ± 0.14	-
4-6	4.47 ± 0.14	-
6-8	4.32 ± 0.14	-
8-10	4.59 ± 0.20	-
10-12	4.19 ± 0.13	-
12-14	5.43 ± 0.17 5.43 ± 0.22	1.03 ± 0.13
14-16	4.70 ± 0.11	-
16-18	4.47 ± 0.17	-
18-20	5.26 ± 0.16 5.50 ± 0.20	0.9 ± 0.12
20-22	4.58 ± 0.19	-
28-30	4.21 ± 0.18	-
38-40	4.54 ± 0.11	-
50-52	4.26 ± 0.16	-
Mean dpm/g*	4.45 ± 0.04	-
Inventory dpm/cm²**	-	5.8

Core 11137

Depth cm	^{210}Pb dpm/g	$^{210}Pb_{excess}$ dpm/g
0-2	7.5 ± 0.2	3.1 ± 0.2
2-4	15.0 ± 0.5 15.0 ± 0.4 15.7 ± 0.5	10.8 ± 0.3
4-6	6.1 ± 0.2	1.7 ± 0.2
6-8	4.78 ± 0.19	0.38 ± 0.19
8-10	4.08 ± 0.15	-
12-14	4.75 ± 0.14	-
16-18	4.31 ± 0.14 4.44 ± 0.16	-
18-20	4.38 ± 0.16	-
20-22	4.46 ± 0.15	-
22-24	4.26 ± 0.14	-
24-26	4.59 ± 0.18	-
34-36	4.75 ± 0.18	-
44-46	4.35 ± 0.18	-
48-50	4.35 ± 0.15	-
Mean dpm/g*	4.42 ± 0.05	-
Inventory dpm/cm²**	-	16.0

Core 11143

Depth cm	^{210}Pb dpm/g	$^{210}Pb_{excess}$ dpm/g
0-1	28.9 ± 0.8	24.5 ± 0.8
1-2	12.7 ± 0.4	8.3 ± 0.4
2-3	8.1 ± 0.2	3.7 ± 0.2
3-4	6.0 ± 0.2	1.6 ± 0.2
4-5	5.5 ± 0.2	1.1 ± 0.2
5-6	5.2 ± 0.2	0.8 ± 0.2
6-7	4.91 ± 0.21	0.51 ± 0.21
7-8	4.60 ± 0.15	0.20 ± 0.15
9-10	4.45 ± 0.16	-
10-11	4.59 ± 0.16	-
11-12	4.81 ± 0.20	-
Inventory dpm/cm²**	-	20.4

Core 11334

Depth cm	^{210}Pb dpm/g	$^{210}Pb_{excess}$ dpm/g
0-1.5	22.4 ± 0.6	18.0 ± 0.6
1.5-3	11.1 ± 0.3	6.7 ± 0.3
3-5	5.73 ± 0.20	1.33 ± 0.20
7-9	4.67 ± 0.15	0.27 ± 0.15
11-13	4.47 ± 0.14	-
15-18	6.88 ± 0.21	-
Inventory dpm/cm²**	-	> 20.1

Core 11145

Depth cm	^{210}Pb dpm/g	$^{210}Pb_{excess}$ dpm/g
0-2	12.1 ± 0.4	7.7 ± 0.4
2-4	6.1 ± 0.2	1.7 ± 0.2
4-6	5.3 ± 0.2	0.9 ± 0.2
6-8	4.33 ± 0.14	-
8-10	4.36 ± 0.20	-
10-12	4.48 ± 0.21	-
12-14	4.17 ± 0.14	-
14-16	4.33 ± 0.14	-
16-18	4.44 ± 0.16	-
18-20	4.72 ± 0.14	-
24-26	4.25 ± 0.14	-
30-32	4.66 ± 0.14	-
42-44	4.58 ± 0.16	-
52-54	4.52 ± 0.16	-
Mean dpm/g*	4.44 ± 0.05	-
Inventory dpm/cm²**	-	10.3

Core 11333

Depth cm	^{210}Pb dpm/g	$^{210}Pb_{excess}$ dpm/g
0-1.5	16.9 ± 0.4	12.5 ± 0.4
1.5-3	12.2 ± 0.3	7.8 ± 0.3
3-5	10.1 ± 0.2	5.7 ± 0.2
5-7	5.4 ± 0.2	1.0 ± 0.2
9-11	4.74 ± 0.15	0.34 ± 0.15
18-19	4.69 ± 0.15	-
19-20	4.33 ± 0.12	-
23-25	4.45 ± 0.16	-
27-30	4.56 ± 0.14	-
33-36	3.85 ± 0.09	-
45-48	3.93 ± 0.09	-
Mean dpm/g*	4.16 ± 0.05	-
Inventory dpm/cm²**	-	> 22.3

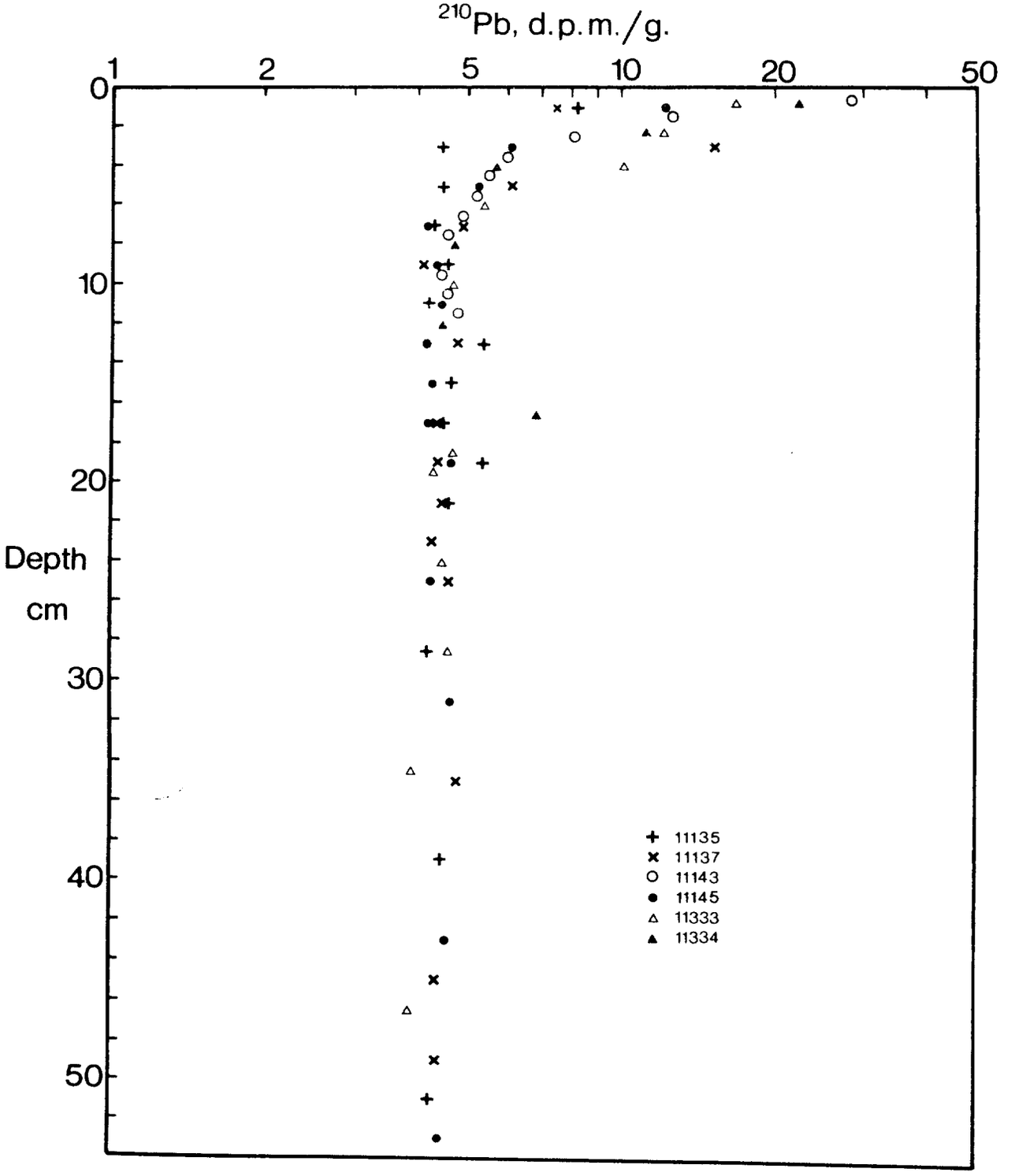

Figure 4.2 Profiles of log (total ^{210}Pb activity) versus depth for the box cores studied.

pointed out that such estimation procedures for $^{210}Pb_{excess}$ do not take account of ^{226}Ra and ^{222}Rn disequilibrium with ^{210}Pb near the sediment/water interface, which may cause an underestimate of $^{210}Pb_{excess}$. Stordahl et al.,(1985) found that such corrections produced no significant differences in three cores where ^{222}Rn data were available. The possible disequilibrium effect is neglected here because no ^{222}Rn data are available.

The general equation for the presence of a tracer in a mixed layer is:

$$\frac{\delta}{\delta t}(\rho.A) = \frac{\delta}{\delta x}\left(\rho.D_B.\frac{\delta A}{\delta x}\right) - \frac{\delta}{\delta x}(\rho.s.A) - \lambda.\rho.A \qquad (1)$$

where A = tracer activity in (d.p.m.).g^{-1},

t = time in y,

ρ = bulk sediment density in g.cm^{-3} (g dry sediment/volume wet sediment),

x = depth in sediment in cm,

D_B = sediment bioturbation coefficient in $cm^2.y^{-1}$,

s = sediment accumulation rate in $cm.y^{-1}$

and λ = tracer decay constant in y^{-1}.

At steady state $\delta/\delta t.(\rho.A) = 0$, and with the assumptions that D_B is constant in the mixed layer and ρ and s are constant, the solution is:

$$A = A_o.\exp\left\{\left[\frac{s - (s^2 + 4\lambda D_B)^{\frac{1}{2}}}{2D_B}\right].x\right\} \qquad (2)$$

with the boundary conditions that $A = A_o$ at $x = 0$, and $A \to 0$ as $x \to \infty$. In the case of a pelagic sediment, s is small so that (2) simplifies to:

$$A = A_o.\exp(-(\lambda/D_B)^{\frac{1}{2}}.x) \qquad (3)$$

An estimate of D_B can therefore be made from the slope of the regression line of ln (activity) versus depth. The steady state assumption is not obvious for this application, but the time over which $^{210}Pb_{excess}$ persists is short (100 years), so that the principal assumption is that bioturbation has resumed. The advantage of this treatment is that it allows a direct comparison with previous work, most of which has used a similar model of bioturbation and estimation procedure. The bioturbation coefficients calculated from the

best-fit lines for each core are shown on Figure 4.3. Cores 11143, 11145, 11333 and 11334 exhibit a continuous decrease of $^{210}Pb_{excess}$ activity with depth and are suitable for such a treatment. Core 11137 has a sub-surface maximum in $^{210}Pb_{excess}$ which has been ignored in the analysis. Similar sub-surface peaks have been ascribed to the feeding modes of particular deep-sea organisms in cases where the organism can be identified (Swinbanks & Shirayama, 1986), or can be inferred from bottom photographs (Smith et al., 1986). By neglecting such a possibility it may be that the value of D_B is overestimated in core 11137. Core 11135 has a low inventory of $^{210}Pb_{excess}$, and those points with an unequivocal $^{210}Pb_{excess}$ level are not distributed regularly with depth. It seems probable that in this case some redistribution of $^{210}Pb_{excess}$ has occurred by the feeding of a large, relatively rare, organism. Many buried GME turbidites show clear evidence of large, rare burrows infilled with pelagic sediment from overlying units at depths greater than those expected from a typical (~ 8 cm) surface mixed layer (e.g. Figure 9 in Appendix 11). In the case of core 11135, however, there is no overlying sediment to provide such a contrast in appearance.

The mixed layer depths, bioturbation intensities, and $^{210}Pb_{excess}$ inventories obtained here are compared with other work where $^{210}Pb_{excess}$ data have been interpreted similarly in Table 4.3. This comparison reveals that the mixed layer depth ranges observed here (7-11 cm), the bioturbation coefficient range (0.08-0.18 cm^2/yr^{-1}) and the $^{210}Pb_{excess}$ inventory range (10-23 dpm/cm^2) are rather similar to those previously estimated in deep-sea Atlantic sediments from a range of locations. This suggests that bioturbation in the surface of turbidite a has been re-established to near-normal levels despite its young age.

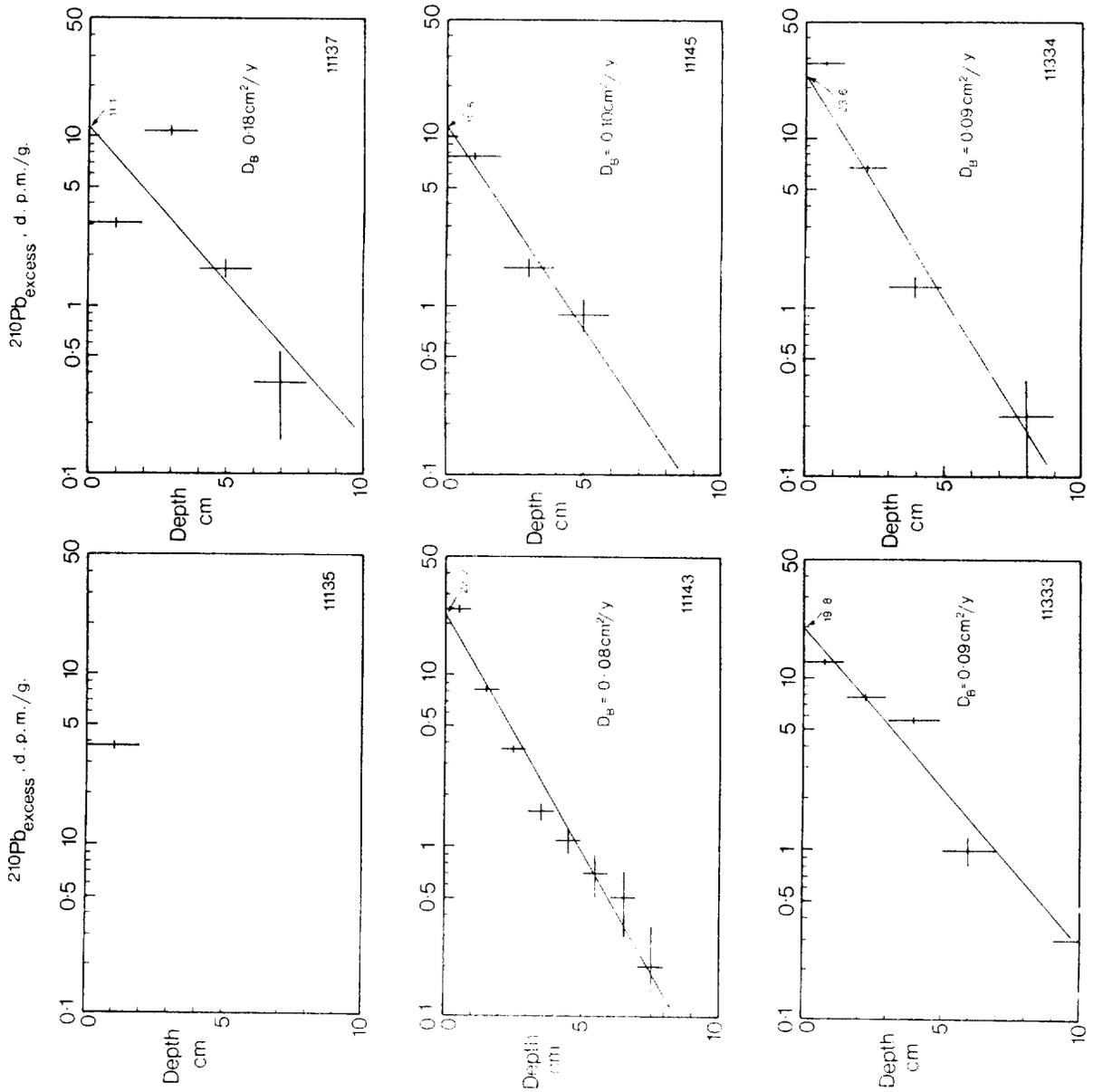

Figure 4.3 Profiles of log ($^{210}Pb_{excess}$ activity) versus depth. The best-fit regression lines and the estimated bioturbation coefficients (D_B) are also shown.

TABLE 4.3 - Reported $^{210}Pb_{excess}$ parameters for deep-sea North Atlantic sediments.

Locality	Core	°N	°W	Water depth (m)	Mixed layer depth (cm)	Bioturbation coefficient D_B $cm^2.yr^{-1}$	Inventory dpm/cm^2	Reference
Central Ridge	527-3	36°49'	33°15'	2705	8	0.19	78	Nozaki et al. (1977)
Bay of Biscay	KG162	47°31'	08°37'	2110	7	0.19	16	Mauviel et al. (1982)
	KG167	47°32'	09°06'	2825	10	0.19	30	Mauviel et al. (1982)
	KG182	47°32'	09°05'	2810	6	0.16	16	Mauviel et al. (1982)
Venezuela Basin (pelagic)	2A	15°07'	69°22'	3950	7	0.10	17	Li et al. (1985)
	2B				10	0.80	15	
	2C				9	0.60	18	
Hatteras Abyssal Plain	77-6-4	~ 30	~ 71	5200	5	0.02	20	Stordahl et al. (1985)
	77-6-2	~ 26	~ 72	5197	5	0.04	20	Stordahl et al. (1985)
Puerto Rico Trench	77-6-11	~ 20	~ 67	8100	5	0.03	8	Stordahl et al. (1985)
Cape Verde Abyssal Plain	76-4-11	~ 22	~ 27	5032	4	0.02	17	Stordahl et al (1985)
	76-4-10	~ 21	~ 25	4660	5	0.04	13	Stordahl et al (1985)
	76-4-9	~ 17	~ 23	3374	9	0.88	29	Stordahl et al (1985)
Madeira Abyssal Plain	161	34°59'	20°30'	5161	8	0.13	33	Kershaw (1985 and pers. comm.)
Great Meteor East	11135#5	31°11'	25°10'	5424	-	-	-	This work
	11137#3	31°26'	24°46'	5428	11	0.18	13	This work
	11143#1	31°13'	25°11'	5423	7	0.08	18	This work
	11145#1	32°08'	24°44'	5424	8	0.10	10	This work
	11133#1	31°18'	25°24'	5438	11	0.17	23	This work
	11134#1	31°31'	24°25'	5438	8	0.09	20	This work

5. SOLID PHASE STUDIES

5.1 Turbidite a

Turbidite a is the uppermost unit over most of the GME area, and the study of this turbidite is important for understanding the record contained in older, buried turbidites. Three box cores from RRS Discovery Cruise 149 and two from Cruise 160 have been analysed comprehensively by XRF techniques. The locations of these cores (11135#5, 11137#3, 11145#1, 11333#1 and 11334#1) are shown on Figure 4.1 and represent north/south and east/west transects of 100 km length in the central GME area. All five cores sampled turbidite a and the remarkable feature of all is the highly consistent composition of the geochemically inert major and minor elements in both the horizontal and vertical (Tables 5.1 to 5.5). The vertical homogeneity of core 11135#5 is illustrated in Figure 5.1 but examination of Tables 5.1 to 5.5 reveals that the horizontal homogeneity is similar. Like many of the GME turbidites, a is fine grained and has a carbonate content of ~ 63% (mainly coccolith calcite).

In four of the five cores a sharp colour contrast in the range 18-22 cm below the sediment/water interface is observed. As discussed in Section 3, this colour change represents the redox discontinuity associated with a progressive oxidation front. The fifth core, 11334#1, has a short (18 cm) turbidite a unit which has been oxidised completely. Further, modelling of the pore water data (Appendix 5) suggests that turbidite a was emplaced around 200 years ago. Despite this short duration, and the low organic content of turbidite a, it is nevertheless possible to discern small signals of post-depositional migration of certain redox-sensitive elements. The identification of these signals in turbidite a where the oxidation front is active is important because similar signals are also found in older, more developed examples which are now inactive (Appendix 12). Here the characteristic locations of these elements with respect to the oxidation front are discussed: the vertical homogeneity of turbidite a (Fig. 5.1) allows this interpretation with some confidence (Appendix 11).

The element which shows the largest signal of redistribution in response to the oxidation front is uranium (Fig. 5.2). The emplacement U content was ~ 2.1 ppm, now seen only in the section 38-52 cm, and this included a small amount of authigenic uranium (~ 1 ppm) above the detrital U content. This detrital U content is ~ 1.2 ppm, and is now seen in the section 0-18 cm. These interpretations are discussed more fully and supported by leaching information

TABLE 5.1 - Core 11333#BX: 31°17.9'N, 25°24.4'W, 5375 m

Depth Interval cm	Major element data, % wt (dry basis)										Trace element data, ppm											
	SiO_2	Al_2O_3	Fe_2O_3	MnO	CaO	K_2O	TiO_2	P_2O_5	LOI	Total	Pb	Ba	I	Rb	Sr	Y	Ni	Co	V	Cr	Cu	Zn
0-1.5	20.52	7.12	2.895	0.064	33.36	1.30	0.379	0.11	32.76	97.21	10	353	73	41	1105	15	27	11	72	41	55	58
1.5-3	20.28	7.10	2.849	0.059	34.62	1.28	0.370	0.12	32.21	97.61	10	492	69	42	1166	16	26	10	70	40	53	58
3-5	20.44	7.11	2.848	0.059	34.15	1.30	0.367	0.11	32.89	97.97	11	492	69	40	1137	15	28	7	72	43	53	56
5-7	19.95	6.81	2.759	0.054	35.18	1.27	0.359	0.12	32.42	97.65	9	605	72	41	1176	15	27	9	67	39	50	56
9-11	19.62	6.71	2.719	0.062	35.10	1.26	0.351	0.11	32.94	97.61	10	647	79	39	1166	15	29	5	66	38	51	58
11-13	19.85	6.67	2.723	0.055	35.42	1.25	0.351	0.12	32.67	97.86	11	656	78	39	1188	15	28	8	67	36	50	56
13-15	19.86	6.71	2.736	0.061	35.25	1.25	0.356	0.13	32.67	97.77	12	662	88	39	1179	15	29	5	67	38	51	58
15-17	19.95	6.75	2.736	0.056	34.99	1.24	0.356	0.13	32.89	97.86	11	648	94	39	1180	15	27	9	66	38	51	57
17-18	19.87	6.62	2.712	0.038	35.08	1.24	0.352	0.12	32.89	97.68	8	654	84	39	1190	15	26	9	67	39	53	56
18-19	19.70	6.55	2.695	0.034	35.14	1.25	0.358	0.11	32.77	97.36	10	596	68	39	1189	14	24	6	74	39	57	57
19-20	19.81	6.64	2.628	0.032	35.33	1.29	0.355	0.12	32.77	97.69	10	629	58	39	1193	15	27	5	75	39	54	57
20-21	19.79	6.59	2.640	0.035	35.42	1.27	0.354	0.11	32.40	97.34	10	616	56	37	1189	14	28	7	69	35	53	57
21-23	19.69	6.61	2.639	0.035	35.15	1.26	0.366	0.12	32.90	97.51	9	612	49	38	1174	14	25	7	68	38	54	56
23-25	19.47	6.51	2.617	0.036	34.79	1.28	0.349	0.12	33.69	97.58	11	622	47	39	1179	14	29	6	69	36	51	55
25-27	19.67	6.49	2.619	0.037	34.95	1.28	0.350	0.11	33.20	97.43	9	629	55	39	1175	14	29	5	68	34	52	56
27-30	19.42	6.54	2.613	0.038	34.72	1.28	0.348	0.13	33.76	97.57	10	618	53	37	1167	14	29	6	67	36	49	54
33-36	19.66	6.55	2.635	0.044	34.58	1.28	0.351	0.11	33.72	97.65	9	624	50	38	1167	14	27	8	68	36	51	56
39-42	19.57	6.52	2.641	0.041	34.87	1.28	0.354	0.11	33.42	97.53	10	621	53	38	1179	15	27	6	68	39	52	55
42-45	19.48	6.52	2.622	0.043	34.84	1.29	0.352	0.12	33.52	97.50	9	658	51	38	1175	14	30	7	71	34	53	54
45-48	19.46	6.49	2.637	0.042	34.83	1.28	0.348	0.13	33.79	97.73	8	604	51	38	1173	14	28	9	70	40	50	56

TABLE 5.2 - Core 11334#BX: 31°30.8'N, 24°25.2'W. 5375 m

Depth Interval cm	Major element data, % wt (dry basis)										Trace element data, ppm											
	SiO_2	Al_2O_3	Fe_2O_3	MnO	CaO	K_2O	TiO_2	P_2O_5	LOI	Total	Pb	Ba	I	Rb	Sr	Y	Ni	Co	V	Cr	Cu	Zn
0-1.5	21.54	7.74	3.14	0.073	32.81	1.32	0.411	0.10	31.45	98.65	12	270	78	44	1096	16	30	10	78	44	56	61
1.5-3	20.34	7.15	2.97	0.067	34.07	1.25	0.386	0.11	32.59	98.93	12	425	60	42	1147	16	28	12	69	38	52	60
3-5	19.83	6.97	2.84	0.064	34.20	1.27	0.370	0.10	33.13	98.77	9	488	57	40	1156	15	29	10	71	40	52	56
7-9	19.62	7.04	2.80	0.070	34.94	1.22	0.366	0.10	32.96	99.12	10	565	59	40	1169	14	29	11	64	38	50	56
11-13	19.49	6.96	2.80	0.092	35.09	1.21	0.359	0.11	32.99	99.10	10	592	59	39	1182	15	38	8	67	40	54	56
15-18	22.34	8.79	3.48	0.073	32.10	1.20	0.424	0.09	30.44	98.94	13	255	58	45	1027	14	33	8	76	58	53	57
18-20	22.04	9.13	3.64	0.060	31.87	1.10	0.414	0.08	30.47	98.80	11	117	50	43	1009	13	29	10	73	66	51	53
20-23	24.32	10.59	4.08	0.104	28.83	1.10	0.448	0.07	28.59	98.13	12	166	37	45	839	13	36	20	71	73	47	[illegible]
25-28	32.45	14.75	5.46	0.160	19.34	1.48	0.594	0.08	22.19	96.50	15	368	36	61	650	17	53	17	91	103	47	[illegible]
31-34	33.26	14.84	5.51	0.182	18.58	1.51	0.606	0.08	21.59	96.16	14	437	43	63	625	18	54	15	91	106	46	[illegible]
36-39	41.52	19.21	6.63	0.192	10.34	1.88	0.741	0.09	16.95	97.55	16	649	57	77	416	20	57	17	108	136	44	[illegible]
41-43	39.05	17.85	6.33	0.179	9.83	1.80	0.728	0.08	17.09	92.94	17	624	95	73	388	20	55	18	106	126	40	[illegible]
43-45	41.11	18.80	6.35	0.116	11.29	1.84	0.726	0.10	17.91	98.24	16	674	163	75	443	20	54	16	106	134	45	31
45-47	38.82	17.47	5.95	0.041	12.21	1.76	0.691	0.11	18.99	96.04	15	677	303	69	467	20	58	11	104	136	62	80
47-48	37.98	16.92	6.04	0.028	13.34	1.74	0.669	0.10	20.22	97.04	14	656	168	69	508	20	38	11	110	134	72	82
48-49	36.96	16.78	5.76	0.028	14.01	1.75	0.661	0.10	20.83	96.88	15	645	155	68	521	19	74	13	147	127	77	83
49-50	36.08	16.54	5.32	0.030	14.28	1.76	0.661	0.09	21.91	96.67	16	669	147	69	527	19	72	15	139	121	61	81
50-52	35.69	16.47	5.28	0.029	14.39	1.81	0.648	0.11	23.45	97.88	15	618	149	67	538	19	71	15	118	117	49	80
52-54	35.11	16.36	5.23	0.031	14.82	1.81	0.641	0.09	22.96	97.05	14	616	145	64	543	17	70	16	98	114	45	76
54-57	35.38	16.18	5.25	0.032	14.11	1.75	0.638	0.09	22.85	96.28	15	628	144	65	549	17	65	14	94	112	43	72

TABLE 5.3 - Core 11135#5BX: 31°11.3'N, 25°10.0'W, 5429 m

Depth Interval cm	Major element data, % wt (dry basis)											Trace element data, ppm										
	SiO_2	Al_2O_3	Fe_2O_3	MnO	MgO	CaO	K_2O	TiO_2	P_2O_5	LOI	Total	Cl	Rb	Sr	Y	Zr	Nb	Ni	Co	V	Cr	Cu	Th
0-2	20.35	6.88	2.75	0.057	1.46	33.47	1.28	0.36	0.11	34.48	100.05	1.42	52	1098	20	75	N.D.	28	10	76	45	52	55
4-6	20.28	6.76	2.73	0.058	1.45	34.77	1.25	0.36	0.11	33.08	99.71	1.50	47	1137	18	79	N.D.	29	12	73	45	52	57
8-10	20.41	6.69	2.71	0.059	1.49	35.25	1.24	0.36	0.11	32.44	99.65	1.46	49	1155	18	79	N.D.	31	10	76	45	54	53
14-16	20.40	6.61	2.69	0.054	1.51	35.32	1.22	0.36	0.12	32.69	99.87	1.57	49	1148	17	78	N.D.	27	10	75	46	57	56
16-18	20.55	6.76	2.72	0.055	1.49	34.97	1.23	0.36	0.12	32.62	99.77	1.52	49	1129	17	73	N.D.	29	10	73	45	54	56
18-20	20.22	6.67	2.61	0.036	1.44	35.16	1.27	0.35	0.11	32.81	99.54	1.47	50	1155	17	79	N.D.	27	8	87	44	59	55
20-22	20.24	6.74	2.64	0.036	1.46	35.13	1.27	0.35	0.12	32.93	99.74	1.65	52	1149	18	72	N.D.	28	7	73	46	54	56
22-24	20.24	6.60	2.65	0.039	1.47	35.33	1.26	0.36	0.12	32.47	99.46	1.52	51	1161	18	74	N.D.	29	8	77	44	55	55
24-26	20.15	6.68	2.65	0.039	1.49	35.78	1.26	0.35	0.11	32.39	99.80	1.61	50	1162	19	73	N.D.	28	9	74	44	54	56
30-32	20.14	6.59	2.64	0.041	1.54	35.45	1.26	0.35	0.11	32.61	99.60	1.68	52	1147	17	76	N.D.	28	10	75	46	57	56
36-38	20.06	6.62	2.64	0.044	1.53	35.34	1.26	0.35	0.11	32.59	99.47	1.55	51	1151	17	81	N.D.	28	9	75	44	53	55
38-40	20.27	6.66	2.67	0.046	1.50	35.59	1.27	0.35	0.12	32.35	99.72	1.53	49	1163	18	80	N.D.	27	8	72	46	55	56
42-44	20.19	6.66	2.64	0.045	1.49	35.53	1.27	0.35	0.10	32.49	99.71	1.62	50	1145	17	80	N.D.	29	10	77	44	53	56
48-50	20.45	6.76	2.67	0.047	1.45	35.64	1.26	0.35	0.11	32.50	100.17	1.57	51	1154	18	72	N.D.	29	10	72	45	55	54
50-52	20.45	6.78	2.64	0.050	1.46	35.11	1.26	0.35	0.11	32.40	99.50	1.70	51	1141	17	75	N.D.	30	11	73	44	53	55

TABLE 5.4 - Core 11137#3BX: 31°25.6'N, 24°46.1'W, 5428 m

Depth Interval cm	Major element data, % wt (dry basis)											Trace element data, ppm										
	SiO_2	Al_2O_3	Fe_2O_3	MnO	MgO	CaO	K_2O	TiO_2	P_2O_5	LOI	Total	Cl	Rb	Sr	Y	Zr	Nb	Ni	Co	V	Cr	Cu	Zn
0-2	20.65	6.99	2.79	0.056	1.46	34.77	1.26	0.36	0.11	32.30	99.60	1.68	51	1133	15	62	14	32	10	81	45	49	56
6-8	20.61	6.93	2.77	0.058	1.43	35.03	1.26	0.36	0.11	32.19	99.60	1.58	49	1155	16	62	14	31	9	78	46	51	56
12-14	20.65	7.06	2.71	0.058	1.43	35.08	1.25	0.36	0.10	32.04	99.65	1.28	48	1161	15	61	14	33	9	77	45	51	58
16-18	20.36	6.71	2.71	0.057	1.49	35.44	1.24	0.35	0.10	32.43	99.78	1.44	43	1164	18	69	15	33	9	74	45	52	57
18-20	19.52	6.43	2.61	0.058	1.65	33.92	1.20	0.34	0.11	34.51	99.25	3.04	51	1091	13	59	14	30	8	74	43	49	54
20-22	20.15	6.72	2.66	0.038	1.43	35.64	1.24	0.35	0.12	32.53	99.78	1.56	49	1164	15	61	15	31	8	90	45	56	57
22-24	19.99	6.68	2.58	0.034	1.45	35.68	1.26	0.34	0.11	33.05	100.03	2.02	50	1166	15	60	14	31	7	79	44	52	56
24-26	20.09	6.67	2.63	0.037	1.42	35.23	1.27	0.35	0.11	32.62	99.29	1.79	49	1176	15	59	14	31	7	76	43	51	56
28-30	20.00	6.72	2.61	0.039	1.51	35.23	1.28	0.34	0.11	33.12	99.78	1.70	50	1171	15	57	14	32	8	77	44	51	56
34-36	19.91	6.59	2.60	0.042	1.47	35.09	1.27	0.34	0.11	33.50	99.79	1.82	50	1157	14	58	15	31	8	79	43	51	55
40-42	20.04	6.66	2.60	0.044	1.44	34.70	1.29	0.34	0.11	33.57	99.63	1.77	50	1142	14	57	14	31	9	78	43	51	55
44-46	19.83	6.65	2.58	0.046	1.53	34.59	1.29	0.34	0.11	33.63	99.42	1.79	46	1132	16	69	14	31	9	76	43	50	55
48-50	19.98	6.72	2.62	0.048	1.40	34.98	1.26	0.34	0.12	32.88	99.26	1.70	50	1168	15	58	14	32	9	75	43	50	55
52-54	20.02	6.69	2.61	0.050	1.46	35.22	1.28	0.34	0.11	33.22	99.86	1.67	50	1159	14	60	15	32	9	75	43	50	55
56-58	19.37	6.52	2.53	0.051	1.57	33.90	1.26	0.33	0.11	34.99	99.46	3.24	51	1091	13	67	15	30	8	74	40	47	52

TABLE 5.5 - Core 11145#1BX: 32°07.6'N, 24°43.5'W, 5424 m

Depth Interval cm	Major element data, % wt (dry basis)											Trace element data, ppm													
	SiO_2	Al_2O_3	Fe_2O_3	MnO	CaO	K_2O	TiO_2	P_2O_5	LOI	Total	Cl	Pb	Ba	I	Rb	Sr	Y	Zr	Nb	Ni	Co	V	Cr	Cu	Zn
0-2	20.84	7.21	2.947	0.066	34.30	1.30	0.398	0.12	31.65	98.83	1.60	10	494	60	45	1177	22	85	12	33	12	82	53	57	60
2-4	20.15	6.82	2.796	0.056	34.78	1.27	0.372	0.12	32.30	98.66	2.12	8	674	67	43	1226	21	80	11	31	11	83	50	55	59
4-6	19.91	6.66	2.754	0.057	35.14	1.23	0.375	0.12	32.36	98.61	1.86	7	814	65	42	1230	20	75	10	33	9	79	49	52	60
6-8	19.84	6.69	2.753	0.057	35.20	1.23	0.364	0.12	32.46	98.71	1.83	8	785	61	42	1231	21	79	12	34	10	78	50	54	59
8-10	20.06	6.72	2.738	0.060	35.78	1.23	0.371	0.13	32.03	99.12	1.68	7	832	68	44	1247	20	80	10	34	9	79	51	54	59
10-12	20.31	6.67	2.741	0.059	35.45	1.23	0.363	0.12	32.33	99.27	1.71	8	817	71	42	1247	20	82	11	33	10	76	49	53	60
12-14	19.71	6.56	2.690	0.060	34.42	1.28	0.356	0.12	33.62	98.82	2.98	7	810	64	40	1225	20	70	10	32	10	76	50	54	58
14-16	19.31	6.41	2.664	0.055	34.77	1.26	0.362	0.12	33.82	98.77	2.70	7	769	78	40	1222	19	75	12	33	10	75	48	52	57
16-18	19.92	6.53	2.717	0.052	35.41	1.22	0.358	0.13	32.45	98.79	1.84	8	822	84	42	1244	20	74	9	32	9	78	49	55	58
18-20	19.69	6.45	2.670	0.032	35.17	1.23	0.358	0.13	32.68	98.43	2.20	8	765	45	42	1248	20	74	12	31	8	88	50	59	59
24-26	19.93	6.45	2.649	0.032	35.45	1.26	0.368	0.12	32.48	98.84	1.95	8	798	53	43	1245	20	79	10	32	8	79	50	55	60
30-32	19.48	6.35	2.626	0.038	34.89	1.26	0.365	0.12	32.63	97.78	2.09	7	804	53	42	1224	18	80	11	31	8	79	49	54	57
36-38	20.06	6.41	2.682	0.042	35.12	1.26	0.373	0.13	32.57	98.44	2.11	7	785	51	42	1229	20	81	11	32	10	80	48	56	58
42-44	19.32	6.32	2.639	0.042	34.91	1.23	0.366	0.12	32.31	97.26	1.90	7	809	57	41	1212	21	80	10	31	8	78	47	53	57
52-54	20.32	6.57	2.684	0.044	34.91	1.26	0.373	0.14	32.14	98.44	1.89	8	789	54	42	1230	19	80	12	32	8	78	49	54	57

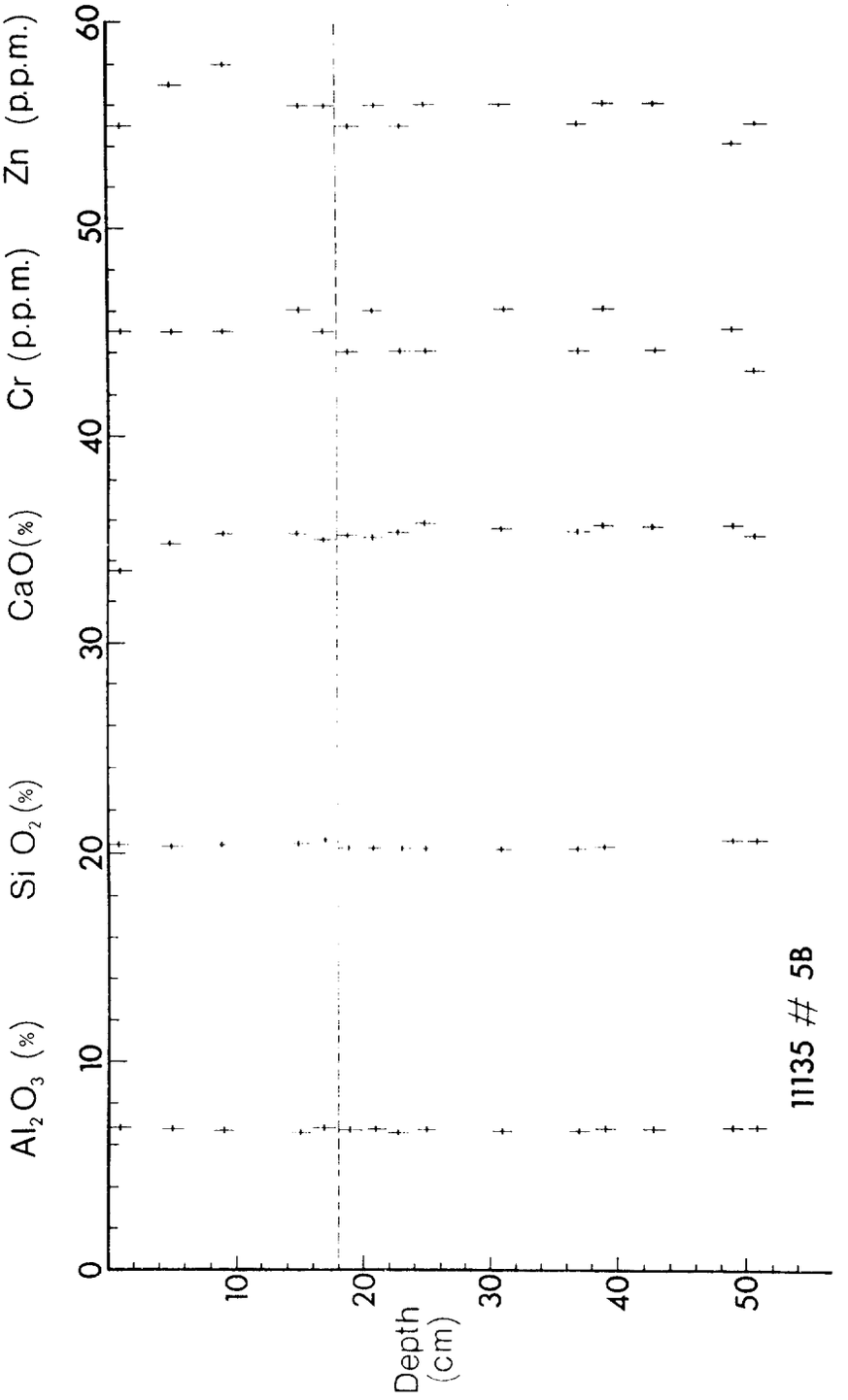

Figure 5.1 Solid phase concentration/depth profiles for major elements SiO_2, Al_2O_3 and CaO and trace elements Cr and Zn for a typical GME box core sampling turbidite a.

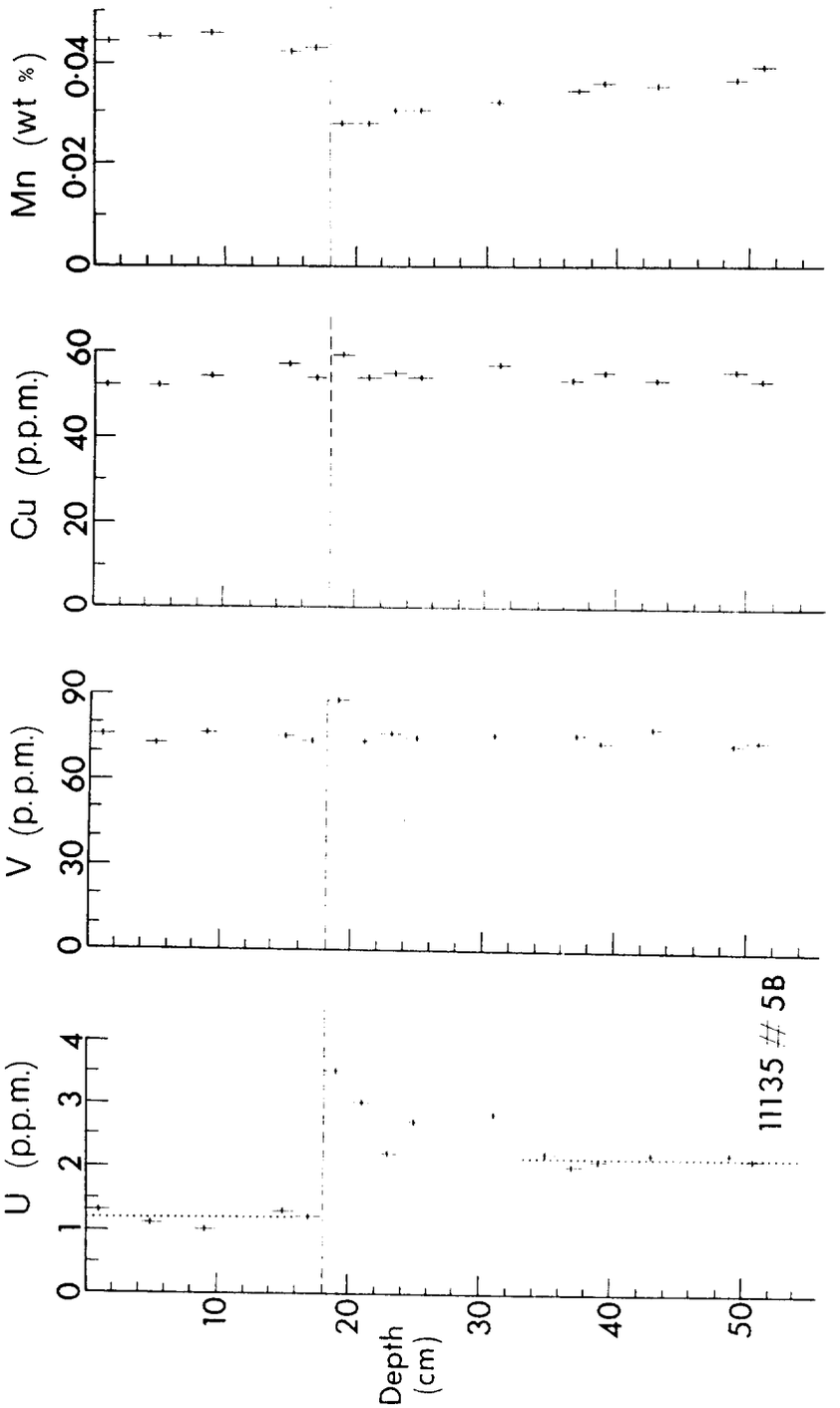

Figure 5.2 Solid phase concentration/depth profiles for redox-sensitive trace elements U, V, Cu and Mn in turbidite a.

elsewhere (Appendix 6). The important point is that authigenic U is repeatedly released to solution in oxic conditions as the front progresses and is immobilised after downwards diffusion into reducing conditions. The consequence is that a peak in U content is observed below the colour change, seen here at depths of 18-32 cm.

The elements V and Cu similarly show an anomalous concentration below the colour change relative to the rest of the core (Fig. 5.2). Although the signals in Figure 5.2 are very small, much larger signals in the concentrations of the same elements are seen in fossil examples at the same relative position. A small authigenic component of those two elements is evidently moved downwards in association with the oxidation front and is located just below the colour change. It is not clear from Figure 5.2 whether this component is derived from the turbidite sediment itself or whether it has diffused down from the sediment/water interface, nor whether the control is by redox change or by association with organic matter. These two elements are, however, immobilised in reducing conditions and therefore are found preserved as peaks in fossil examples in a similar fashion to U (Appendix 12). Measurements of Cu in solution in pore waters extracted from turbidite a show a flux of Cu from oxic waters and the immobilisation of copper below the oxidation front (Appendix 15).

Whereas the elements just discussed migrate downwards from oxic to post-oxic conditions, Mn migrates upwards from reducing conditions to be immobilised in oxic conditions. Data presented in Appendix 7 demonstrate that the source of the pore water Mn(II) seen in Figure 3.6 is a manganese oxyhydroxide concentration located near the former pelagic surface below turbidite a. The detailed pore water and solid-phase Mn from two box cores sampling turbidite a are illustrated in Figure 5.3. The oxic zone above the colour change has the highest Mn content where Mn(II) has been precipitated as Mn oxyhydroxide. Below the colour change, the Mn content of the sediment again increases linearly with depth. This is interpreted as representing an uptake of Mn(II) from pore water solution in reducing conditions by the calcite of the sediment to form a manganous carbonate (Appendix 7).

It will be evident that Mn which has been precipitated in oxic conditions will become thermodynamically unstable when it is subjected to reducing conditions on burial under later turbidites. This aspect is discussed further in Appendices 7 and 12.

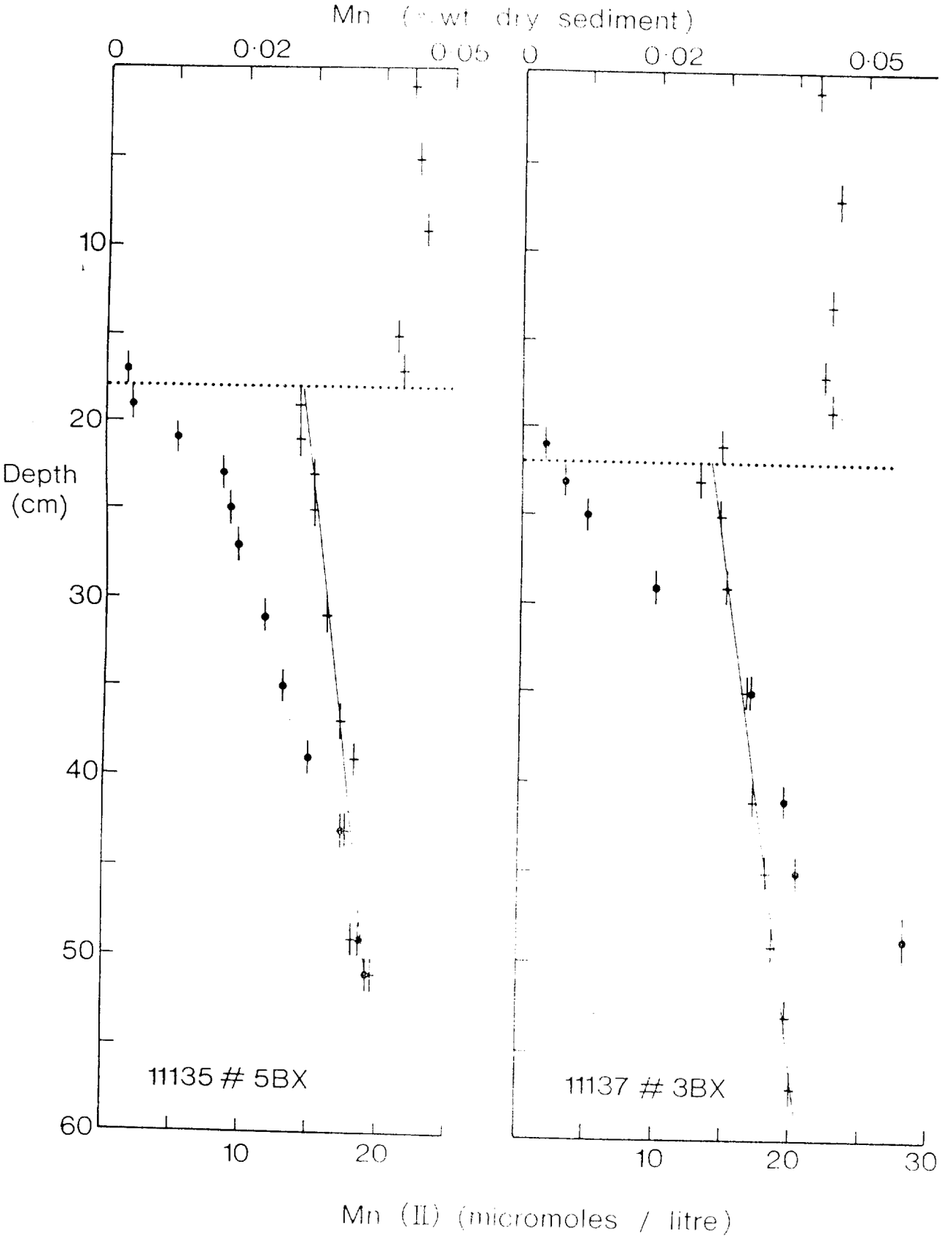

Figure 5.3 Solid phase (crosses) and pore water (dots) data for Mn in two box cores sampling turbidite a.

5.2 Turbidite a1

Turbidite a1 was emplaced about 10,000 years ago (Weaver & Kuijpers, 1983; Appendix 4), and in the eastern part of the GME area is overlain by only a thin veneer of pelagic sediment and turbidite a. In this area the active oxidation front is observed to be oxidising the C_{org} of turbidite a1 (Appendix 4). The major differences between turbidites a and a1, besides time of emplacement, are that turbidite a1 was much more organic-rich on emplacement (1.5% versus 0.5% C_{org}) and has a lower carbonate content (25% versus 63% $CaCO_3$). The high C_{org} content of turbidite a1 gives the unoxidised section of the sediment a distinct olive-green colour. The carbonate content of a1 is low by comparison with most other GME turbidites emplaced over the past 300,000 years (Appendix 12).

Despite these differences between a1 and a, the same redistributions of the same elements U, V, Cu and Mn are observed relative to the colour change associated with the oxidation front (Fig. 3.4). The signals in metal concentration of a1 are much better developed, however, because of the longer operation of the oxidation front and the higher levels of authigenic metals originally introduced. The observation that similar redistributions have occurred in two different and dissimilar turbidites attests to the generality of the oxidation front mechanism and gives a basis for interpretation of the concentration depth profiles in older, buried turbidites where the oxidation front mechanism is no longer active. The contrast in the solid phase composition of the two turbidites is reflected in the concentrations of Mn, Fe, Cu and Ni in solution in the pore waters of the two turbidites (Appendix 15).

5.3 Buried turbidites

Two aspects of the work already described, the pore water environment of the sediment column below the oxidation front and the redistributions of redox-sensitive elements in response to the oxidation front mechanism, are necessary to interpret the solid phase evidence from longer cores which contain buried turbidites. Below the oxidation front the pore water condition is generally post-oxic (i.e. containing neither free oxygen nor sulphide (Berner, 1981)) for a considerable depth, so that in buried turbidites the oxidation front mechanism is no longer active. Nevertheless, the effects of relict oxidation fronts are obvious in organic-rich (> 0.5% C_{org}) turbidites as a lighter colour tone in the upper parts. This gives the opportunity to compare the compositional data observed in deeper turbidite examples with the data from

turbidites a and a1 where the oxidation front process is active.

This comparison is made in Appendix 12, where a representative 10 m core (D10688) is intensively sampled and analysed. It is clear from this work that significant early diagenetic redistribution of the elements Fe, Mn, P, Co, Cu, Ni, U, V and Zn has occurred. This suite of elements is greater than that identified in the active cases of turbidites a and a1, presumably because some of the turbidites in core 10688 have high C_{org} contents and experienced bottom water oxidation for periods of a few tens of thousands of years to develop more marked redistributions. The greater length of some of the turbidites also means that there is a long section unaffected by oxidation from which to characterise the emplacement levels of most elements. Again, the remarkable consistency in the vertical of most turbidites is evident.

The data of Appendix 12 have also been utilised in a further study, not reproduced here (de Lange et al, 1987). This further paper concerns the geochemical characteristics and provenance of the sediments giving rise to the GME turbidites. It demonstrates that the geochemical data define three separate groups of turbidites: (i) organic rich, with high C_{org} and S, (ii) 'volcanic', with high TiO_2 contents and (iii) calcareous, with high $CaCO_3$ and Mn levels. The organic rich turbidites (a, a1, d, e, f, h, s, s1 and u) are postulated to have arisen from the productive area of the NW African continental margin to the east and south-east of GME. The 'volcanic' turbidites (b, b1, d1, g, i, n, o and p) are thought to have an oceanic island source to the east, probably the Canaries and Madeira. Calcareous turbidites (j, l, r and s2) are thought to have originated from the Great Meteor-Cruiser Seamount Chain to the west.

6. STUDIES OF URANIUM GEOCHEMICAL BEHAVIOUR IN THE GME TURBIDITES

A phenomenon of uranium relocalisation was first identified in deep-sea turbidite sediments by IOS on the DoE high-level radioactive waste disposal research programme (Appendices 1 & 6). The sediments of the GME area are mainly made up of turbidites, interbedded with thin units of pelagic sediments. Many of the turbidites have a high organic content with which is associated an extra (authigenic) uranium content. Following emplacement of a turbidite on the GME abyssal plain, the organic carbon of the turbidite is progressively oxidised by downwards diffusion of oxygen from bottom waters (see Section 3). In parallel, the authigenic uranium associated with the organic-rich sediments is mobilised in oxic conditions by the passage of the front, and migrates to reducing (anoxic) conditions below the front. As a consequence, a peak in uranium concentration forms below the oxidation front and continually moves and is augmented so long as the front is active (Fig. 6.1). These uranium peaks are preserved as relict structures when the turbidite is buried by subsequent emplacements. This behaviour is clearly important as a natural analogue for waste disposal studies. Consequently, various other aspects of these uranium concentration/depth profiles have been investigated.

6.1 Reproducibility of uranium peaks in individual turbidites

The sediments of the GME area have been studied by comparison of conventional piston cores (10-15 metres in length) taken by IOS and Dutch workers. As a result of the number and spread of piston cores available, the stratigraphy of the area 30°-33°N, 23°-26°W is well known and the stratigraphic correlations over the past 250,000 years have been demonstrated to be very good (Weaver & Kuijpers, 1983). A series of piston cores was collected by IOS for geochemical studies on RRS Discovery Cruise 149 in 1984. These cores formed a rough N-S transect in the centre of the GME area (Fig. 6.2).

Samples were taken from two individual turbidites, d and e, in which relict uranium peaks had been found previously. Uranium and organic carbon concentration/depth profiles are presented for these two turbidites in Figures 6.3 and 6.4. The colour changes in the turbidites, which represent the levels in the turbidites achieved by the oxidation fronts when active, are chosen as the reference levels on the depth axes. It can be seen (Figs. 6.3 & 6.4) that the uranium peak shapes and positions, together with the steps in organic carbon content, are consistent in all cores. This is remarkable since the cores are up to 110 kilometres distant from each other (Fig. 6.2). It may

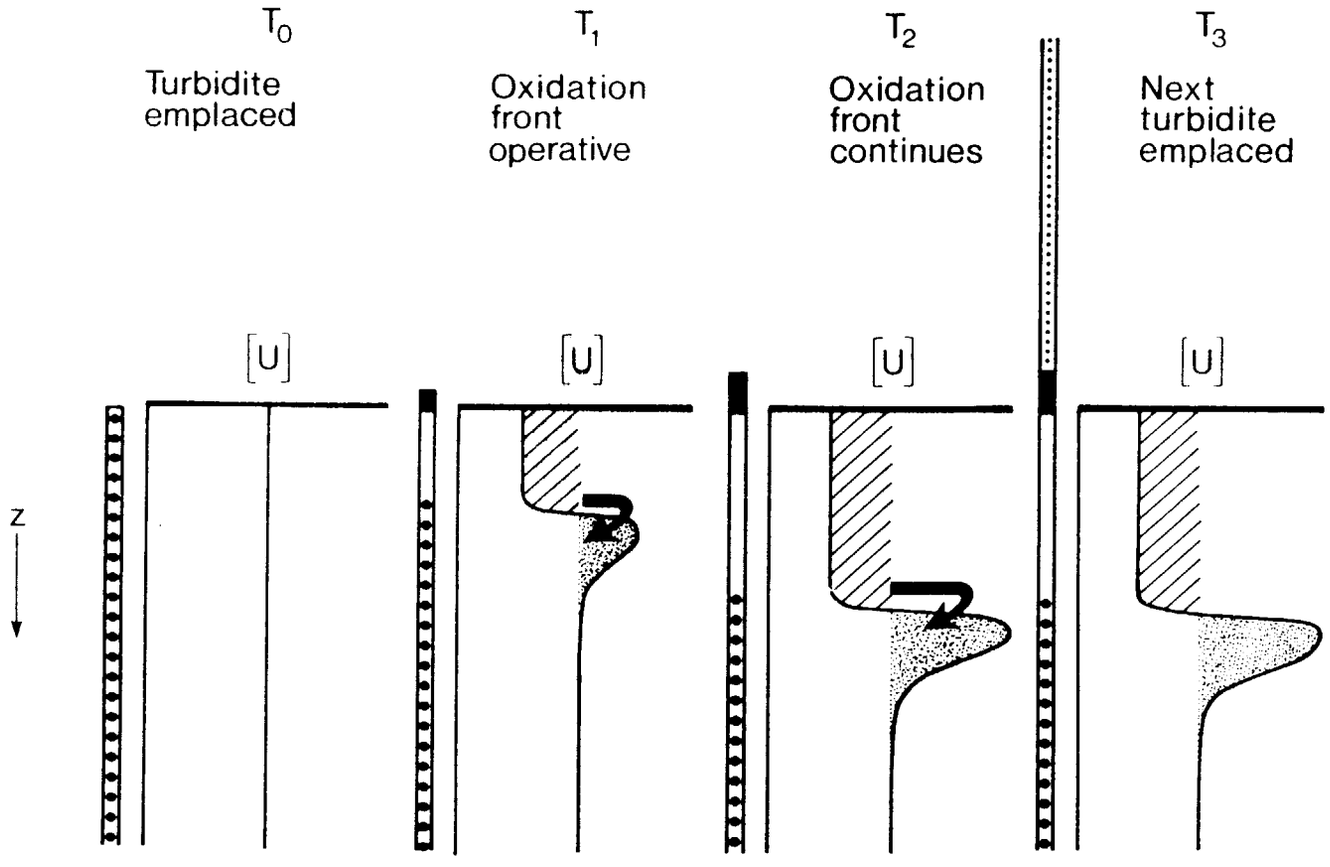

Figure 6.1 A representation of the sequence of events following turbidite emplacement: T_o - turbidite emplaced with constant uranium concentration in the vertical; T_1 - oxidation front releases authigenic uranium in oxic conditions, which is then immobilised in anoxic conditions as a peak; T_2 - oxidation front continues to progress downwards enlarging peak; T_3 - emplacement of a new turbidite stops the process, and uranium peak is now relict.

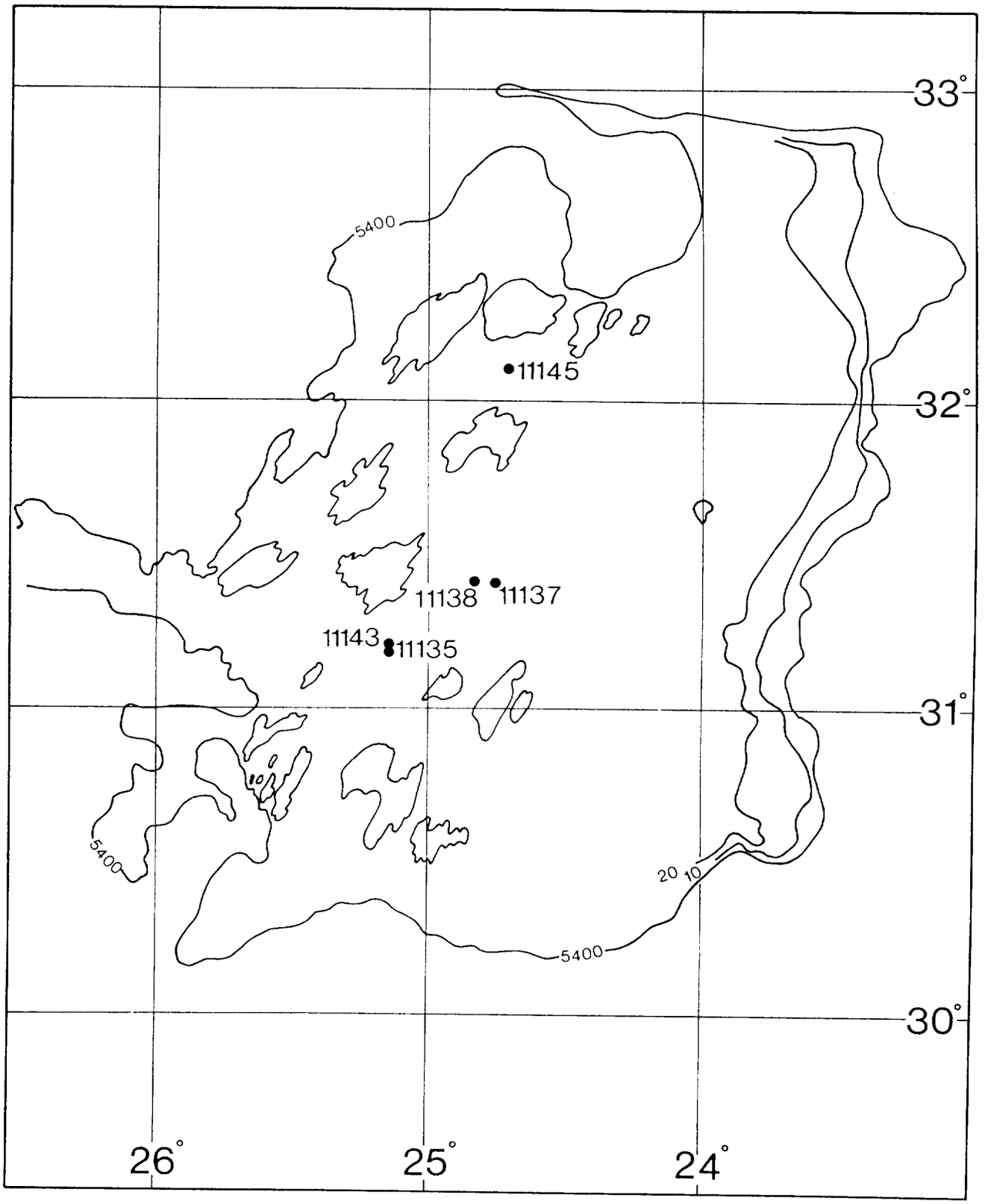

Figure 6.2 Map of the GME area showing the positions of the piston cores used in the study of reproducibility of uranium peaks in individual turbidites.

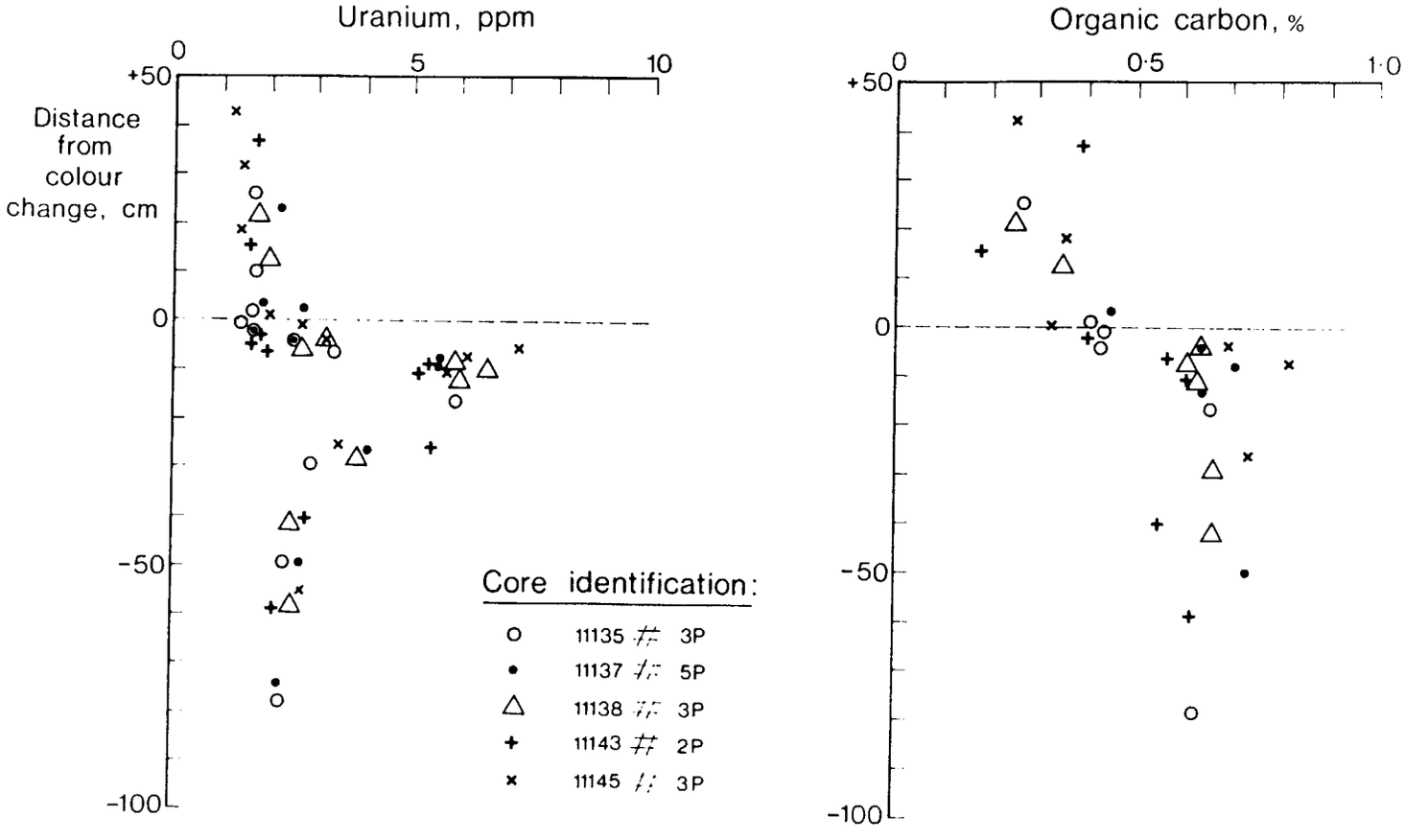

Figure 6.3 The reproducibility of the positioning of the uranium peak relative to the relict oxidation front (colour change) in five different piston cores sampling turbidite a. The zero reference level is the colour change in each core. The five cores are up to 100 km apart.

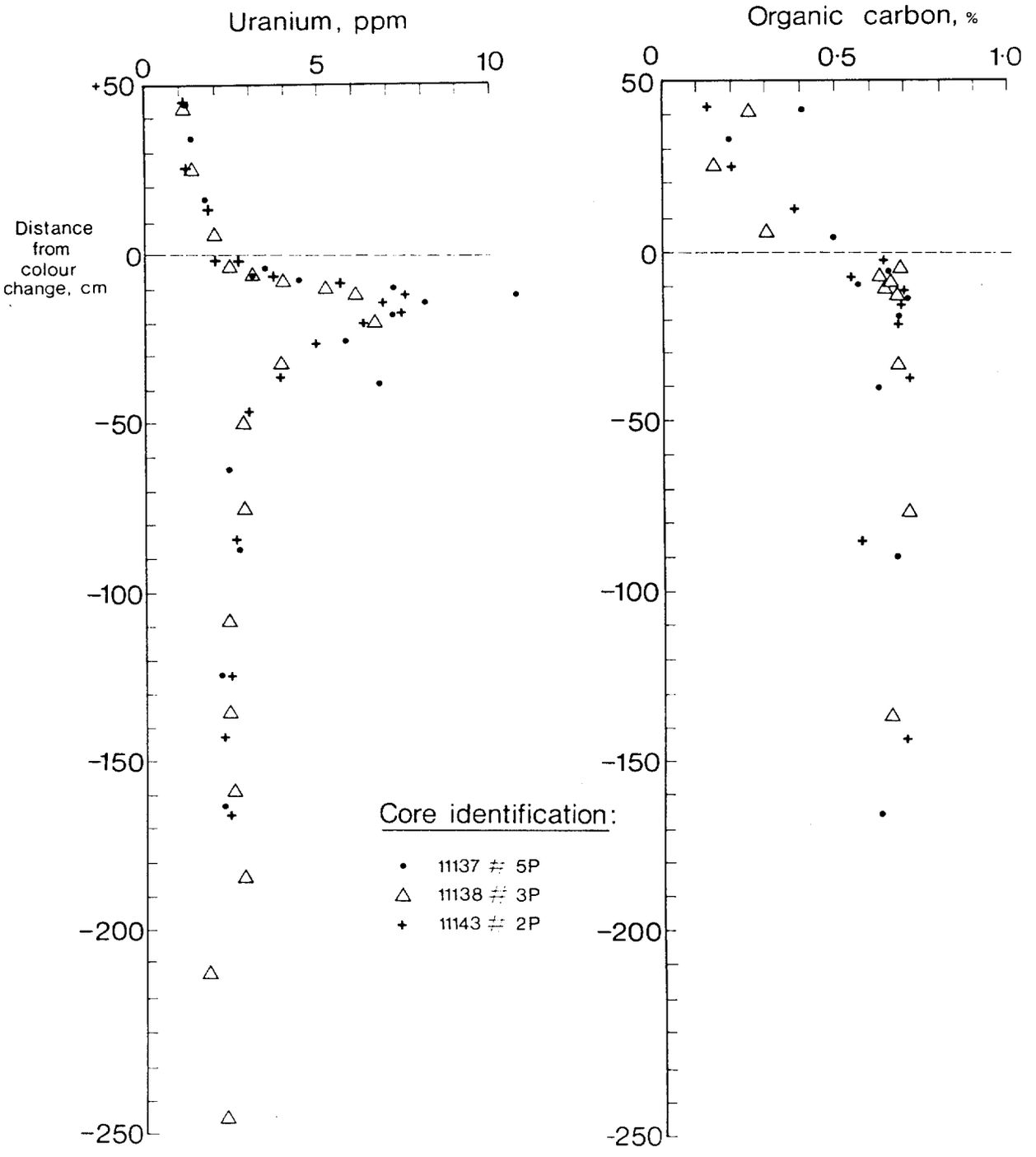

Figure 6.4 A similar treatment to that of Figure 6.3 for three cores sampling turbidite e.

be concluded that the uranium peak in a buried turbidite is localised in a 20-cm thick zone starting about 5 cm below the colour change.

6.2 The record of uranium peak formation through time

The stratigraphic investigations by Weaver and Kuijpers (1983) concern the past 250,000 years, which is a limit imposed by the sediment accumulation rate of the GME area and the length of normal piston cores. One such core, 10688, was used by Colley and Thomson (1985), here as Appendix 6, to define the uranium behaviour over this time period. In recognition of the fact that conventional piston cores cannot retrieve material from the 30 m depth envisaged for radioactive waste disposal, the NEA Sea-bed Working Group co-ordinated an internationally-funded cruise to take extra long cores. This cruise took place in 1985 on the French research vessel Marion Dufresne and the French "STACOR" device was used to recover cores up to 35 m long.

As UK participants on the cruise, IOS obtained sediment samples from two cores from the GME area (cores MD10 and MD24). The uranium concentration/depth profile of core MD24 is illustrated in Figure 6.5 along with the provisional stratigraphy (P.P.E. Weaver, personal communication). To obtain maximum detail for the analytical effort involved, the data for Figure 6.5 begin where the profile of core 10688 (Appendix 6) left off. It is evident that the characteristic uranium profile shapes in individual turbidites (Fig. 6.1) can still be discerned in Figure 6.4, despite the fact that the oldest turbidites in core MD24 were emplaced up to 750,000 years ago. Further discussion of these data may be found in Appendix 14. This finding of uranium immobility has clear implications for the potential behaviour of artificial radionuclides buried at similar depths for similar periods.

6.3 Mechanism of uranium fixation in reducing conditions

The paper in Appendix 6 discusses the conflicting theories as to why sediments with an anoxic pore water environment are often enriched with authigenic uranium. That paper suggests that redox conditions are the important control rather than the sediment organic content, based on stratigraphic interpretations of the location of uranium peaks in relation to the oxidation fronts in thin turbidites at GME; in these cases, the U peaks are displaced out of the organic-rich turbidites into the underlying pelagic units which have lower organic contents. Such a mechanism implies that uranium is soluble as a U(VI) complex in oxic conditions, but insoluble as a U(IV) species

Figure 6.5 (following page)

Stratigraphic log and uranium profile for the lowest part (12 m to 30 m) of "Marion Dufresne" core 24. Oxygen isotope stages and age estimates (P.P.E. Weaver, pers. comm.) are shown. Positions of relict oxidation fronts, seen as colour changes in the sediment, are marked by dashed lines on the log and by arrows on the profile. Uranium peaks with a similar disposition to the fronts may be seen throughout the sediment section back to approximately 750,000 years.

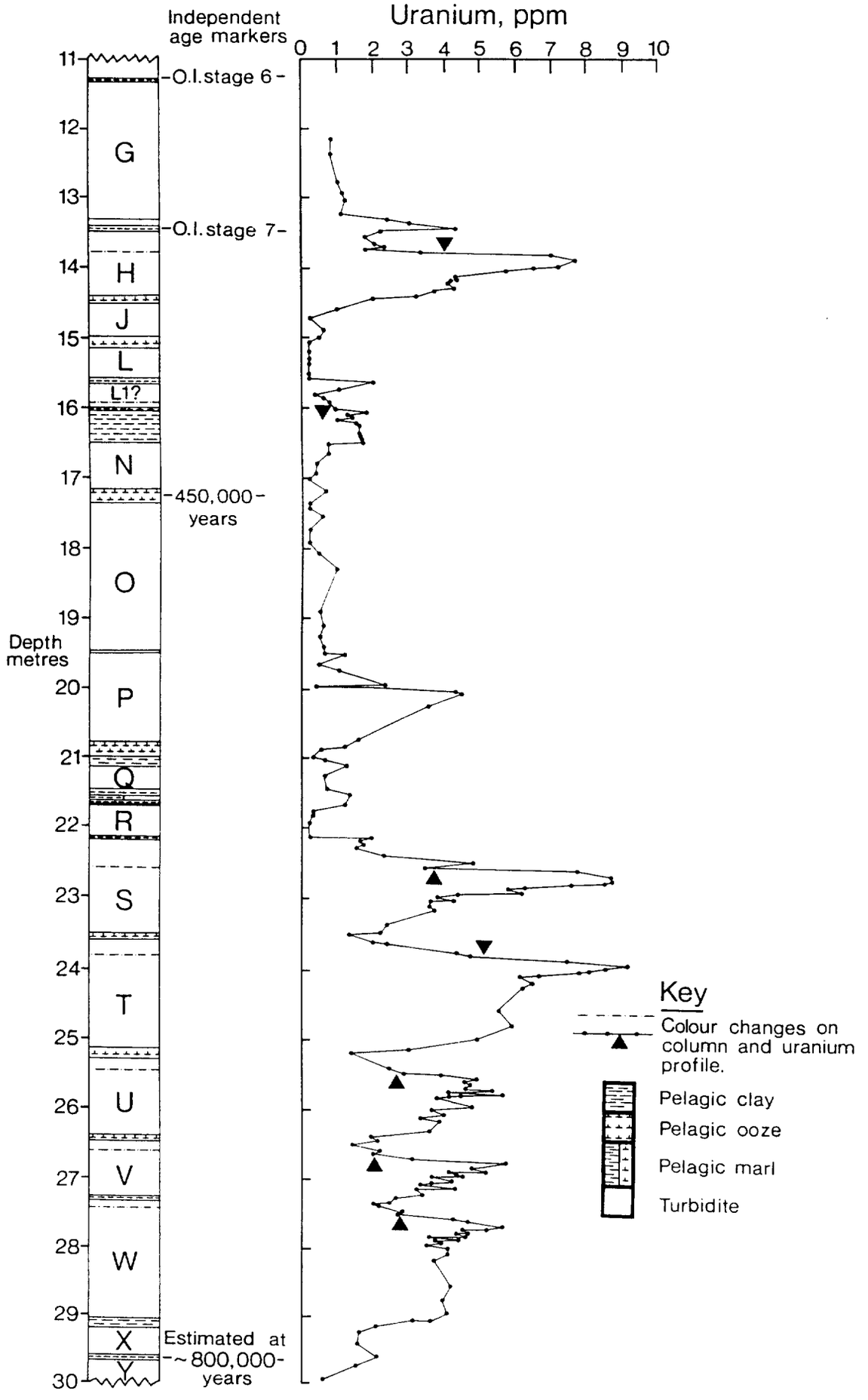
Independent age markers
Uranium, ppm
0 1 2 3 4 5 6 7 8 9 10
11
12
13
14
15
16
17
18
19
20
21
22
23
24
25
26
27
28
29
30
Depth metres
-O.I. stage 6-
-O.I. stage 7-
-450,000- years
Estimated at ~800,000- years
G
H
J
L
L1?
N
O
P
Q
R
S
T
U
V
W
X
Y
Key
Colour changes on column and uranium profile.
Pelagic clay
Pelagic ooze
Pelagic marl
Turbidite

in reducing conditions.

It was originally envisioned that this redox mechanism could be demonstrated directly by separate analyses of the U(IV) and U(VI) oxidation states in the solid phase. A method is available to make such an analysis for phosphorites, which are complex carbonate fluoroapatite rocks that generally have high uranium contents (Kolodny & Kaplan, 1970). This method gave apparently sensible results in our hands when used on phosphorite samples (Table 6.1), but failed on GME sediment samples. Several added safeguards against uranium oxidation on dissolution were added (low temperature, inert nitrogen atmosphere throughout early processing stages, sparging of all reagents with nitrogen before use) but no convincing evidence of the presence of U(IV) was found. This work was effectively terminated by the requirement to send the IOS inert atmosphere facilities on the 1985 Marion Dufresne cruise for pore water work, following which they required extensive maintenance through damage incurred in return transit.

Table 6.2 illustrates a complete analysis of a sediment sample obtained with the phosphorite method at a stage when all precautions were being taken. It can be seen that very little U(IV) is determined (the cupferron precipitate analysis) and that most of the labile uranium is present in the filtrate as U(VI). It remains a possibility that some oxidation of the trace quantities of U(IV) occurs on dissolution by other redox-sensitive cations present at much greater concentrations (e.g. Fe(III) or Mn(IV)), but at present this line of investigation does not appear likely to be fruitful.

6.4 In-situ diffusion of uranium

The presence of well-preserved uranium peaks in MD24 (Fig. 6.5), which have persisted for as long as 750,000 years, suggests at least qualitatively that there has been little mobility of uranium. To obtain a more quantitative estimate from this data, it is necessary to make an estimate of the degree to which this deepest peak has broadened and spread since it was emplaced. Assuming that all peaks were formed in identical conditions, a systematic increase of peak width downcore might indicate increased mobility of U with age. In fact, the turbidites differ in thickness and in source material, causing a variation in U peak size. Inspection of Figure 6.5, and similar data from more recent turbidites, indicates that no direct correlation exists between depth in the core and peak width. This implies that diffusion is not of overriding importance in controlling the uranium behaviour even on these long time scales.

Table6.1 - ANALYSIS OF URANIUM OXIDATION STATES IN PHOSPHORITE 2220 CI FOR COMPARISON WITH A TOTAL ANALYSIS

Sample Description	U ppm	Th ppm	U/Th	$^{234}U/^{238}U$ activity ratio	$^{230}Th/^{232}Th$ activity ratio
Total analysis	91 ± 1	3.6 ± 0.3	25 ± 2	0.97 ± 0.01	78 ± 5
Partial analyses					
1*	33 ± 1	0.88 ± 0.21	38 ± 1	0.79 ± 0.03	24 ± 6
2**	31 ± 1	2.03 ± 0.41	15 ± 3	1.35 ± 0.06	110 ± 22

* Analysis of cupferron precipitate (UIV)
** Analysis of filtrate from cupferron precipitate (UVI)

Table 6.2 - ANALYSIS OF URANIUM OXIDATION STATES IN A BULK SAMPLE FROM BELOW THE OXIDATION FRONT IN TURBIDITE A_1 FOR COMPARISON WITH A TOTAL ANALYSIS

Sample Description	U ppm	Th ppm	Th/U	$^{234}U/^{238}U$ activity ratio	$^{230}Th/^{232}Th$ activity ratio	^{230}Th dpm/g	^{234}U dpm/g	$^{230}Th_{excess}$ dpm/g
Total analysis	5.09 ± 0.15	9.3 ± 0.3	1.83 ± 0.08	1.05 ± 0.03	2.91 ± 0.05	6.61 ± 0.15	4.00 ± 0.12	2.61 ± 0.19
Partial analyses								
1*	0.20 ± 0.01	1.91 ± 0.12	9.6 ± 0.8	0.99 ± 0.10	5.24 ± 0.32	2.43 ± 0.09	0.15 ± 0.01	2.28 ± 0.09
2**	3.35 ± 0.16	1.68 ± 0.16	0.50 ± 0.05	1.11 ± 0.05	6.99 ± 0.66	2.86 ± 0.15	2.77 ± 0.13	0.09 ± 0.20
3***	1.41 ± 0.06	4.50 ± 0.38	3.19 ± 0.31	1.13 ± 0.06	0.94 ± 0.09	1.03 ± 0.09	1.18 ± 0.05	-0.15 ± 0.10
4****	4.96 ± 0.17	8.1 ± 0.4	1.63 ± 0.10	1.11 ± 0.06	3.21 ± 0.28	6.32 ± 0.20	4.10 ± 0.14	2.22 ± 0.24

* Analysis of cupferron precipitate (UIV)
** Analysis of filtrate from cupferron precipitate (UVI)
*** Analysis of residue from initial orthophosphoric acid leach (detrital U)
**** 1 + 2 + 3 for comparison with total analysis

In order to set an upper limit on the effective diffusion coefficient it is only necessary to decide on the maximum decrease in peak height that can have occurred. It seems unlikely, for instance, that the uranium peak in turbidite s (age about 600,000 years) was very much higher at the time of its formation than it is now; the assumption has therefore been made that this peak height has not been depleted by more than a factor of two since deposition. This appears to be a reasonably conservative criterion, and its use permits the calculation of an upper estimate to the possible mean value of the effective uranium diffusion coefficient in deep GME sediments.

To illustrate the sensitivity of the peak height to the effective diffusion coefficient, a coefficient of 10^{-12} cm^2 sec^{-1} would give a reduction of the turbidite s peak height of only 0.1% in 600,000 years, while a value of 10^{-10} cm^2 sec^{-1} would imply that this peak is now only 23% of its initial height. Using Fick's treatment of diffusion, it can be shown (Crank, 1956) that the maximum concentration of a substance diffusing away from a source layer (half-thickness h) in an isotropic medium is given by

$$C_t = C_o(\text{erf } (h/2(Dt)^{0.5})) \qquad (1)$$

where C is the concentration,
C_o is the initial concentration,
D is the (constant) diffusion coefficient,
erf is the error function
and t is the time.

Taking h = 20 cm, t = 600,000 years and the ratio of initial and final concentrations to be 2, as discussed above, it is clear that the effective in-situ diffusion coefficient cannot be greater than 2×10^{-11} cm^2 sec^{-1}, and may well be considerably less.

This value is valid for the GME sediment column below about two metres, assuming that the existing sub-oxic pore water environment is not disturbed. Introduction of a waste package may cause the environment to become more oxidising. This is dependent in turn on the redox buffering capacity of the sediment. Both of these factors are still unknown, but an increase in oxidising conditions could promote increased mobility of U as a U(VI) complex, and considerably alter the in-situ diffusion coefficient.

Given this reservation, however, the measurement of an in-situ diffusion coefficient for an important waste nuclide is a major advance in knowledge of

the system, and provides a bench-mark for evaluation of the reliability of laboratory measurements. The observation that uranium-mobilising conditions have not predominated for any significant period within the past 750,000 years is also notable, since it indicates that under natural conditions the redox state of the system is stable and predictable. A useful further extension of this study can be made by investigating the concentrations of daughter isotopes within the uranium decay series around the oldest peaks. Any departures from the expected secular equilibrium concentration profiles would indicate enhanced migration of the appropriate daughter, under the real geochemical conditions of the deep sedimentary environment.

7. THE GEOCHEMISTRY OF MANGANESE AT GME

Manganese, of all the major metallic elements, exhibits the most dramatic relocations during early sediment diagenesis. Under anoxic conditions, a large proportion of the manganese deposited with a sediment is thermodynamically unstable and migrates as Mn(II) along a pore water concentration gradient towards oxic conditions. In oxic conditions a complex manganese oxyhydroxide phase precipitates as a coating on sediment particles. Manganese oxyhydroxide has a large surface area and is an effective sorption agent for many other cations such as Co, Ni and Ra. In more reducing sediments than those at GME, such oxyhydroxide coatings can amount to several percent by weight of the total sediment in a thin, near-surface zone. A special study of manganese was undertaken to examine its behaviour in the GME sediments (Appendix 7).

The work reported in Appendix 7 revealed that, although there was clear evidence of the manganese recycling behaviour outlined above, a competing process was that of uptake of Mn(II) from pore water solution by calcite surfaces. Thus, although manganese oxyhydroxide does form in the restricted (< 1 m) oxic zone of the uppermost sediment column, about half of the total manganese at depth is calcite-associated. When a GME sediment surface with an oxyhydroxide concentration is buried by the emplacement of a new turbidite, it becomes metastable, Mn(II) is produced and diffuses up through the new turbidite towards oxic conditions. A remarkable fact is that the constant turbidite compositions in the vertical allow the uptake of Mn(II) by calcite to be discerned as a slope in the overall Mn content of a particular turbidite, greatest at the base and least at the top. The preservation of this gradient suggests that there is no well developed solid/solution equilibrium, and that once sorbed the manganese(II) is fixed by calcite.

The process above clearly acts so as to limit the diffusion of Mn(II) in the sediments and also limit the magnitude of near-surface manganese oxyhydroxide localisations. The possible effect of a similar calcite uptake on other elements of interest in a radioactive waste context is not clear, although Am, $Np(V)O_2^+$ and $Pu(V)O_2^+$, for example, have high affinities for natural carbonate surfaces in sea water solution (Shanbhag & Morse, 1982; Keeny-Kennicutt & Morse, 1984, 1985).

8. GEOCHEMICAL STUDIES ON PORE WATER ADVECTION

The sediments of the Madeira Abyssal Plain, in common with most deep-ocean sediments, are very fine-grained. Flow of pore water relative to the solid phase (advection) is therefore restricted. For the purpose of the present study, it is important to determine if such flow occurs since advection could, in principle, result in an enhanced radionuclide transport rate away from a buried waste container. Some vertical flow is, of course, consequent upon the process of compaction; the flow rates due to this process are, however, very limited and of little significance in the present context.

It is known that convective flow occurs in sediments close to mid-ocean ridges. The formation of new crust consequent upon sea floor spreading at these ridges ensures that the geothermal gradient is high and the overlying sediment cover is thin, thus facilitating advective flow. As the newly-formed crust moves away from its point of formation it cools and accumulates a thicker burden of sediment, and heat-flow measurements indicate that convective processes become insignificant fairly rapidly. Most heat-flow measurements on abyssal plains show a linear geothermal gradient in the upper sediments indicating that conductive, rather than convective, processes predominate.

Occasionally, however, non-linear temperature profiles are reported. Noel (1984) has reviewed the possible reasons for such profiles and suggests six alternative causal mechanisms in addition to vertical advection. It is thus clear that the existence of such profiles is by no means conclusive evidence that vertical advection is present. However, the possible sensitivity of radionuclide transport rates to advective events requires that the possibility of such events at the study site be closely investigated. This report is concerned with geochemical approaches to this problem; direct methods (pore pressure measurement) have also been used; they are detailed in the corresponding geophysics report and are summarised in Appendix 9.

The geochemical advection studies are detailed in Appendices 8 and 10. These studies took advantage of the proximity of DSDP site 608 to the King's Trough Flank study site. Appendix 10 details the derivation of an expression for the effect of advection on the highly linear calcium and magnesium profiles observed in pore water measurements from site 608. It was concluded that these profiles are incompatible with a vertical pore water advection of greater than 0.006 cm yr^{-1}. This contrasts with an estimate based on heat flow measurements at a nearby site of 52 cm yr^{-1} (Appendix 10). It must be concluded that the geochemical measurements are totally incompatible with such advective velocities

at site 608; the time to establish steady-state in a diffusive slab 400 m thick is in the order of several hundred years so that no such events can have occurred within this interval.

This work rested on the fortuitous fact that site 608 shows highly linear profiles over great depth intervals. The study given in Appendix 8 seeks to extend this to more normal profiles by investigating the effect of advection on the profiles generated by a diagenetic numerical model. This model gives nitrate and oxygen profiles in the upper few centimetres. Although these profiles do not begin to show advective effects until the imposed advective velocity exceeds about 15 cm yr^{-1}, it is interesting to note that above this velocity the model indicates that very considerable distortions are imposed on the predicted pore water profiles. Thus it is possible to state that the higher values of advective velocity postulated on the basis of heat flow measurements are totally incompatible with the presence of chemical gradients of the type almost universally observed in deep ocean sediments.

Since the intensive study site at GME exhibits linear nitrate and oxygen profiles over the upper 30 cm or so, it is possible to utilise the mathematical treatment of Appendix 10 to determine the minimum detectable advection threshold compatible with this data. This evaluation indicates that these profiles would lose linearity detectably at vertical advective velocities of the order of 1 cm yr^{-1}.

The ESOPE exercise produced pore water data over a depth range of about 30 m, two orders of magnitude greater than the shallow data mentioned in the previous paragraph. The ESOPE report evaluates these observations in terms of pore water advection; this evaluation will not be repeated here. However, it may be pointed out that the sensitivity of the linear profile technique for the detection of pore water advection is directly proportional to the thickness of the depth interval over which the pore water profile is linear. Consequently, the linear profiles obtained from the ESOPE data do not appear to be compatible with vertical advective velocities of much greater than 10^{-2} cm yr^{-1}, using the treatment and assumptions of Appendix 8.

Although these estimates are valid for the time and place of measurement, a problem arises in their application to radionuclide migration prediction. The natural system has a very short 'memory' for advective events. The pore pressure, for instance, falls to zero within days of the cessation of flow, while the linear chemical profiles observed in the shallow GME data would be re-established within about two years of the end of an event (Appendix 10).

The deeper ESOPE profiles would be slower to recover but, even so, would be fully re-established after a few hundred years of zero flow. Thus, the geochemical data presented so far do not speak directly to the problem of detecting sporadic events in the past, or predicting any such events in the future.

It is, however, possible to draw inferences from the solid phase data on uranium presented in Section 6. This data shows that the distribution of uranium within each turbidite unit follows a consistent pattern related to the diagenetic processes which move uranium in oxidising conditions. Since these distributions are preserved in units which were laid down up to 750,000 years ago, it does not seem possible that oxidising conditions can have obtained within this sediment column during that time. This implies that a downward advective flow of oxygenated bottom water into the sediments, sufficient to erase the uranium record by oxidation, cannot have occurred since emplacement. Unfortunately, this argument cannot be used to rule out upward flow, since that would presumably not mobilise the uranium from the solid phase, but the data do indicate a relatively stable redox environment at the GME site during the last few hundred thousand years. It is true to say that none of the geochemical data obtained during the present study appear to indicate that vertical pore water advection is likely to be important in the prediction of radionuclide migration rates at the GME study site, although the assumptions made in the treatments of Appendices 8 and 10 should be borne in mind when evaluating the significance of this observation.

9. NATURAL SCAVENGING PROCESSES IN THE NORTH-WEST ATLANTIC: NARES ABYSSAL PLAIN

Early in the course of the contract, a study was made of short cores from the Nares Abyssal Plain. Previous work suggested that the clays of this area are relatively free of biogenic material and consist of two major and readily recognised types. These are grey clays rapidly sedimented from distal turbidity currents, and red clays slowly sedimented from oceanic nepheloid layers. This work is reported as Appendix 2. Despite their colour differences, it was demonstrated that the two major clay types have a closely similar detrital composition and probably have the same terrigenous origin. Sediment accumulation rates were established by the $^{230}Th_{excess}$ technique for some red clay sections and found to be in the range 0.3-0.7 $g.cm^{-2}.10^{3}yr^{-1}$, rather higher than previous estimates. These rates allowed application of a model whose output was, first, an estimate of the detrital composition of the red clays and, second, an estimate of the authigenic flux of the metals Mn, Fe, Cu, Co, Ni, Zn, V and the rare earth elements. This authigenic flux component was applicable to the eastern Nares Abyssal Plain over the past 100,000 years. Comparison with other reported studies suggested that authigenic fluxes from the water column are variable both between and within ocean basins by about an order of magnitude for some elements.

An important aspect of this work not discussed in Appendix 2 arises from a finding reported in Appendix 1. In Appendix 1, a core was investigated which contained a single thin turbidite in a brown clay section. A severe alteration halo was observed below the turbidite in which the brown clay had been converted to a red colour. This was interpreted as a reduction effect caused by the turbidite, and it was demonstrated that the elements Mn, Co, Ni and Cu had been mobilised from the originally brown clay and that Fe had been added. This suggests that much of the authigenic component quantified in Appendix 2 will be unstable towards reducing conditions and will migrate in the sedimentary column. Further work along these lines would clearly be relevant to the radioactive waste management research programme, as it allows study of the movement of common elements in sediments under natural conditions over long time periods. The concentration of effort on GME sediments later in the project caused this aspect to be laid aside.

10. SUMMARY

1. Early in the present research, geophysical evidence showed that sedimentation on the Madeira Abyssal Plain (GME study site) was dominated by sporadic horizontal inflow of sediments originally deposited in shallower water (turbidites). **Section 2.**

2. The geochemistry of these sediments was investigated using a variety of sampling techniques. Particular emphasis was placed on obtaining samples of good vertical resolution (box corer) and chemical integrity (in-situ pore water sampler). It was shown by comparison of these techniques that alkalinity and uranium concentrations in pore waters alter when core samples are decompressed on recovery. In-situ samples are necessary for such studies. **Section 3.**

3. The sediments at GME were found to be anoxic at unexpectedly shallow depth, even though the overall metabolic activity was comparable to that found at oxidising sites at similar water depths. This novel finding was traced to differences in the vertical distribution of metabolic activity, consequent upon the turbidite-dominated sedimentary regime at GME. **Section 3.**

4. It was shown that an oxidation front developed at the top of each turbidite and progressed downward with time as the organic carbon of the turbidite was metabolised. This process is terminated when the turbidite unit is isolated from bottom water by the arrival of the next turbidite. **Sections 3 and 5.**

5. Existing steady-state models were not adequate to deal with this situation and an alternative numerical model of the processes involved was developed. This model was based on the concept of a progressive oxidation front. **Sections 3 and 5.**

6. The model was used to calculate the development of the redox field with time in a newly-emplaced turbidite. This calculation was used to estimate an emplacement age for the most recent turbidite. **Section 3.**

7. The uppermost turbidite at GME was emplaced only a few hundred years ago. Despite this recent age, it is clear that the intensity of near-surface sediment mixing is similar to that observed elsewhere in the deep sea, and that bioturbation is not the dominant control on the oxidation front mechanism. **Sections 3, 4 and 5.**

8. The 10 km² intensive study area lies in a part of the Madeira Abyssal Plain in which the last turbidite (a) attains a depth of several decimetres. Conditions at this site appear to correspond closely to those found at stations up to 100 km away in this area of the Plain. Minor differences are observed along an east-west axis; these appear to be related to changes in turbidite thickness which are, in the main, systematic and predictable. **Sections 3 and 5.**

9. The progressive oxidation front consists of a very strong redox gradient compressed into a relatively short vertical interval. The migration of various redox-sensitive elements has been studied by taking advantage of the effects of this unusually intense redox field. This not only provides required information on the development of the naturally occurring redistributions and conditions but also provides natural analogues for radionuclide species. **Sections 3, 5 and 6.**

10. The distribution of such elements in the solid phase of relict (buried) turbidites was investigated. Significant redox-mediated relocation of iron, manganese, phosphorus, cobalt, copper, nickel, uranium, vanadium and zinc was found and the specific reasons for the observed distributions were studied. **Section 5.**

11. Uranium is the most strikingly active element studied, being mobile in oxidising conditions and fixed under the reducing conditions which obtain at depth at GME. Relict uranium enrichments which appear to have persisted with little or no movement of U for three-quarters of a million years in these sediments have been identified. To the extent that natural uranium can be regarded as an analogue for waste uranium, this indicates that the latter is expected to be trapped within the sediment if the environment remains in its natural reducing state. **Section 6.**

12. Three compositional groups for GME turbidites have been identified on the basis of comprehensive solid-phase elemental composition data. These groupings have been used to assign tentative source areas for 21 sampled turbidites. **Section** 5.

13. It has been demonstrated that a specific interaction of manganese with calcite operates so as to limit both the overall diffusion rate of Mn(II) and the magnitude of near-surface manganese oxyhydroxide localisations. **Section 7.**

14. Geochemical results do not support the present existence of significant active vertical pore water flow within GME sediments and place some constraints on the nature and intensity of any such flow in the past few hundred thousand years. However, evidence is not yet available to rule out completely the possibility that some vertical or horizontal flow might occur at or near the GME study site. **Section 8.**

15. Many other uncertainties remain. The extent to which the emplacement of waste containers might be capable of modifying the natural redox field is totally unknown, and obviously very important. A number of potentially significant diagenetic reactions which are known to occur at the GME site also remain to be studied. **Section 11.**

16. Early diagenetic relocations of the elements Fe, Mn, P, Co, Cu, Ni, U, V and Zn have been identified in the GME sediments. Further natural analogue studies are possible but have not been pursued so far. **Sections 5, 6 and 9.**

11. FUTURE STUDIES

The earlier sections indicate the considerable progress which has been made in understanding the natural geochemical processes within the GME sediments. However, some processes at GME, which may well be important in the prediction of waste radionuclide behaviour, are not yet understood. In some cases, anomalous results challenge our present level of understanding. In other instances, problems have simply not yet been addressed. Further work, listed here in no particular order, is therefore required.

1. A significant uncertainty concerns the redox stability of the GME sediments with respect to the disturbance caused by a large-scale emplacement operation. The effect of this is almost totally unknown. Because the mobility of many elements is strongly dependent on oxidation state, it is important to predict the redox implications of the emplacement operation. This requires a reliable prediction of the waste matrix and containment and the near-field products, both stable and radioactive. Given this information, work is then necessary to determine the in-situ redox buffer capacity of the sediments in order to predict migration rates in the presence of a large-scale disposal operation.

2. The reasons for the observed anomalous redox status of turbidite b are unclear. Low levels of nitrate and of oxygen appear within turbidite b, well below the sharp oxidation front and apparently isolated from oxygenated bottom water by turbidite a, a layer containing no oxygen. Either this is a relict feature, in which case an explanation is required for the slow oxygen diffusion, or there is some mechanism active which can occasionally by-pass the reduced layer and transport oxygen to unusually large depths. Possibilities are bioturbation or horizontal movement of pore water within turbidite b. Of all the GME sites studied geochemically, this phenomenon appears most marked in the 10 x 10 km box identified by DoE for closest examination.

3. The reason for the apparent absence of significant reduction of pore water sulphate in the buried organic-rich layers at GME is unknown. Our present understanding would predict that the high organic content of turbidite a1 might well result in sulphate reduction in the turbidite b region; instead, this layer is anomalously oxidising.

4. Silicate-consuming diagenetic reactions are found within certain layers at GME. Large variations in dissolved silica profiles occur with depth. Maxima exceed 600 x 10^{-6} molar, while intermediate minima can be less than 25% of this value. This strongly suggests that diagenetic reactions occur in certain pelagic intervals; these reactions are assumed to consume silica from solution in forming new silicate minerals. What are the products, and are the reactions quantitatively significant in the present context?

5. Deeper reactions occur at this site, which liberate ammonia and consume sulphate. Flux calculations indicate that simple reduction of sulphate at depth is probably not the only process active. This phenomenon would be difficult to study without deeper samples but, since it occurs at and below the disposal depth, it should not be ignored.

6. As more information is obtained giving better precision and detail to the description of the environment, better mathematical models of the system's geochemical processes will be required. These will need to be developed in close association with the field measurements and geochemical interpretation in order to ensure the relevance of the model to the true situation and, conversely, the applicability of the data to the modeller's needs.

7. The work with uranium indicates that this natural multivalent element is mobile under oxygenated conditions but is not subject to substantial movement in a moderately reducing environment. The characteristic uranium profile shapes also suggest that such uranium profiles which have been in place for long periods (hundreds of thousands of years) can be used for the study of uranium daughter mobility. These and other isotopes of the same elements are also found as daughters of artificial actinides.

8. The processes at the sediment-water interface are not adequately understood. This is not strictly limited to the GME area, since radionuclides released to the ocean by any process, intended or accidental, will be influenced by removal and cycling processes associated with the biology, mineralogy and geochemistry of the sediment-water interface. Consequently, work on these processes is relevant to existing disposal

practices, to the accident scenario and to any release which may occur at the GME site itself. Field tests involving benthic incubation experiments are required and these should be related further to water column studies using pump samplers and sediment traps.

9. It has been demonstrated that Mn(II) uptake by calcite is acting to retard manganese mobility in the GME sediments. The possibility that calcite might have a specific effect on actinide uptake, as is suggested by laboratory studies, is important and requires further investigation.

REFERENCES

ALLER, R.C. & DEMASTER, D.J. 1984 Estimates of particle flux and reworking at the deep-sea floor using $^{234}Th/^{238}U$ disequilibrum.
Earth and Planetary Science Letters, 67, 308-318.

BENDER, M.L. 1971 Does upward diffusion supply the excess manganese in pelagic sediments?
Journal of Geophysical Research, 76, 4121-4215.

BERNER, R.A. 1981 A new geochemical classification of sedimentary environments.
Journal of Sedimentary Petrology, 51, 359-365.

BERGER, W.H. & HEATH, G.R. 1968 Vertical mixing in pelagic sediments.
Journal of Marine Research, 26, 134-143.

BONATTI, E., FISHER, D.F., JOENSUU, O. & RYDELL, H.S. 1971 Post-depositional mobility of some transition elements, phosphorus uranium and thorium in deep-sea sediments.
Geochimica et Cosmochimica Acta, 35, 189-201.

BOOTY, B. (Ed.) 1985 Status report on research at the Institute of Oceanographic Sciences related to the possible disposal of radioactive waste on or beneath the seafloor: April 1979 - March 1984.
Institute of Oceanographic Sciences, Report, No. 204, 333pp.

BOUDREAU, B.P. 1986a Mathematics of tracer mixing in sediments: I - Spatially-dependent, diffusive mixing.
American Journal of Science, 286, 161-198.

BOUDREAU, B.P. 1986b Mathematics of tracer mixing in sediments: II - Non-local mixing and biological conveyor-belt phenomena.
American Journal of Science, 186, 199-238.

COCHRAN, J.K. 1985 Particle mixing rates in sediments of the eastern equatorial Pacific: evidence from ^{210}Pb, $^{239,240}Pu$ and ^{137}Cs distributions at MANOP sites.
Geochimica et Cosmochimica Acta, 49, 1195-1210.

CRANK, J. 1956 The mathematics of diffusion.
Oxford: Clarendon Press, 347pp.

DE LANGE, G.J. JARVIS, I. & KUIJPERS, A. 1987 Geochemical characteristics and provenance of late Quaternary sediments from the Madeira Abyssal Plain, North Atlantic.
In, Geology and geochemistry of abyssal plains, (ed. P.P.E. Weaver and J. Thomson).
Oxford: Blackwells for Geological Society. (Special Publication 31) (in press)

DEMASTER, D.J. & COCHRAN, J.K. 1982 Particle mixing rates in deep-sea sediments determined from excess ^{210}Pb and ^{32}Si profiles.
Earth and Planetary Science Letters, 61, 257-271.

DRUFFEL, E.R.M., WILLIAMS, P.M., LIVINGSTON, H.D. & KOIDE, M. 1984 Variability of natural and bomb-produced radionuclide distributions in abyssal red clay sediment.
Earth and Planetary Science Letters, 71, 205-214.

FROELICH, P.N., KLINKHAMMER, G.P., BENDER, M.L., HEATH, G.R., CULLIN, D., DAUPHIN, P., HAMMOND, D., HARTMAN, B. & MAYNARD, V. 1979 Early oxidation of organic matter in pelagic sediments of the eastern equatorial Atlantic: suboxic diagenesis.
Geochimica et Cosmochimica Acta, 43, 1075-1090.

GOLDBERG, E.D. & KOIDE, M. 1962 Geochronological studies of deep sea sediments by the ionium/thorium method.
Geochimica et Cosmochimica Acta, 26, 417-450.

GUINASSO, N.L. & SCHINK, D.R. 1975 Quantitative estimates of biological mixing rates in sediments.
Journal of Geophysical Research, 80, 3032-3034.

KEENY-KENNICUTT, W.L. & MORSE, J.W. 1984 The interaction of $Np(V)O_2^+$ with common mineral surfaces in dilute aqueous solutions and seawater.
Marine Chemistry, 15, 133-150.

KEENY-KENNICUTT, W.L. & MORSE, J.W. 1985 The redox chemistry of $Pu(V)O_2^+$ interaction with common mineral surfaces in dilute solutions and seawater.
Geochimica et Cosmochimica Acta, 49, 2577-2588.

KERSHAW, P.J. 1985 ^{14}C and ^{210}Pb in NE Atlantic sediments: evidence of biological reworking in the context of radioactive waste disposal.
Journal of Environmental Radioactivity, 2, 115-134.

KOLODNY, Y. & KAPLAN, I.R. 1970 Uranium isotopes in seafloor phosphorites.
Geochimica et Cosmochimica Acta, 34, 3-24.

LI, W.Q., GUINASSO, N.L., COLE, K.H., RICHARDSON, M.D., JOHNSON, J.W. & SCHINK, D.R. 1985 Radionuclides as indicators of sedimentary processes in abyssal Caribbean sediments.
Marine Geology, 68, 187-204.

LYLE, M. 1983 The brown-green colour transition in marine sediments: a marker for the Fe(III)-Fe(II) redox boundary.
Limnology and Oceanography, 28, 1026-1033.

MAUVIEL, A., NGUYEN, H.V., CHESSELET, R., SIBUET, M., YOKOYAMA, Y. & AUFFRET, G. 1982 Etude des variations des taux de bioturbations par la spectrometrie gamma non-destructive (GeHP), dans trois zones sedimentaires de l'Atlantique Nord, a 2000 m et a plus de 4000 m de profondeur.
Bulletin de l'Institut de Géologie du Bassin d'Aquitaine, No. 31-32, 257-274.

MÜLLER, P.J. & MANGINI, A. 1980 Organic carbon decomposition ratio in sediments of the Pacific manganese nodule belt dated by ^{230}Th and ^{231}Pa.
Earth and Planetary Science Letters, 51, 96-114.

NOEL, M. 1984 Origins and significance of non-linear temperature profiles in deep-sea sediments.
Geophysical Journal of the Royal Astronomical Society, 76, 673-690.

NOZAKI, Y., COCHRAN, J.K., TUREKIAN, K.K. & KELLER, G. 1977 Radiocarbon and ^{210}Pb distribution in submersible-taken deep-sea cores from Project FAMOUS.
Earth and Planetary Science Letters, 34, 167-173.

OFFICER, C.B. 1982 Mixing, sedimentation rates and age dating for sediment cores.
Marine Geology, 46, 261-278.

PENG, T-H., BROECKER, W.S. & BERGER, W.H. 1979 Rates of benthic mixing in deep-sea sediment as determined by radioactive tracers.
Quaternary Research, 11, 141-149.

PENG, T-H. & BROECKER, W.S. 1984 The impacts of bioturbation on the age difference between benthic and planktonic foraminifera in deep-sea sediments.
Nuclear Instruments and Methods in Physics Research, B5, 346-352.

SCHINK, D.R. & GUINASSO, N.L. 1979 Redistribution of dissolved and adsorbed materials in abyssal marine sediments undergoing biological stirring.
American Journal of Science, 278, 687-702.

SEARLE, R.C., SCHULTHEISS, P.J., WEAVER, P.P.E., NOEL, M., KIDD, R.B., JACOBS, C.L. & HUGGETT, Q.J. 1985 Great Meteor East (distal Madeira Abyssal Plain): geological studies of its suitability for disposal of heat-emitting radio-active wastes.
Institute of Oceanographic Sciences, Report, No. 193, 162pp.

SHANBHAG, P.M. & MORSE, J.W. 1982 Americium interaction with calcite and aragonite surfaces in seawater.
Geochimica et Cosmochimica Acta, 46, 241-246.

SMITH, J.D. & HAMILTON, T.F. 1984 Improved technique for recovery and measurement of polonium-210 from environmental materials.
Analytica Chimica Acta, 160, 69-77.

SMITH, J.N., BOUDREAU, B.P. & NOSHKIN, V. 1986 Plutonium and ^{210}Pb distribution in northeast Atlantic sediments: subsurface anomalies caused by non-local mixing.
Earth and Planetary Science Letters, 81, 15-28.

STORDAL, M.C. JOHNSON, J.W., GUINASSO, N.L. & SCHINK, D.R. 1985 Quantitative evaluation of bioturbation rates in deep ocean sediments: II - Comparison of rates determined by ^{210}Pb and ^{239,240}Pu.
Marine Chemistry, 17, 99-114.

SWINBANKS, D.D. & SHIRAYAMA, Y. 1986 High levels of lead-210 in the deep-sea infaunal xenophyophore Occultammina profunda.
Nature, 320, 354-358.

TUREKIAN, K.K., COCHRAN, J.K. & DEMASTER, D.J. 1978 Bioturbation in deep-sea deposits: rates and consequences.
Oceanus, 21, 34-41.

WEAVER, P.P.E. & KUIJPERS, A. 1983 Climatic control of turbidite deposition on the Madeira Abyssal Plain.
Nature, 306, 360-363.

WEAVER, P.P.E. & ROTHWELL, R.G. 1987 Sedimentation on the Madeira Abyssal Plain over the last 300,000 years.
In, Geology and geochemistry of abyssal plains, (ed. P.P.E. Weaver and J. Thomson).
Oxford: Blackwells for Geological Society. (Special Publication 31).
(in press)

WEAVER, P.P.E., SEARLE, R.C. & KUIJPERS, A. 1986 Turbidite deposition and the origin of the Madeira Abyssal Plain.
Pp. 131-143 in, North Atlantic Palaeoceanography, (ed. C.P. Summerhayes and N.J. Shackleton).
Oxford: Blackwells for Geological Society, 473pp. (Special Publication 21).

LIST OF APPENDICES (not included)

1. COLLEY, S., THOMSON, J., WILSON, T.R.S., HIGGS, N.C. 1984 Post-depositional migration of elements during diagenesis in brown clay and turbidite sequences in the north-east Atlantic. Geochimica et Cosmochimica Acta, 48, 1223-1235.

2. THOMSON, J., CARPENTER, M.S.N., COLLEY, S., WILSON, T.R.S., ELDERFIELD, H. & KENNEDY, H. 1984 Metal accumulation rates in north-west Atlantic pelagic sediments. Geochimica et Cosmochimica Acta, 48, 1935-1948.

3. TOOLE, J. THOMSON, J., WILSON, T.R.S., BAXTER, M.S. 1984 A sampling artefact affecting the uranium content of deep-sea porewaters obtained from cores. Nature, 308, 263-266.

4. WILSON, T.R.S., THOMSON, J., COLLEY, S., HYDES, D.J., HIGGS, N.C. & SØRENSEN, J. 1985 Early organic diagenesis: the significance of progressive subsurface oxidation fronts in pelagic sediments. Geochimica et Cosmochimica Acta, 49, 811-822.

5. WILSON, T.R.S., THOMSON, J., HYDES, D.J., COLLEY, S., CULKIN, F. & SØRENSEN, J. 1985 Oxidation fronts in pelagic sediments: diagenetic metal-rich layer formation. Science, 232, 972-975.

6. COLLEY, S. & THOMSON, J. 1985 Recurrent uranium relocations in distal turbidites emplaced in pelagic conditions. Geochimica et Cosmochimica Acta, 49, 2339-2348.

7. THOMSON, J., HIGGS, N.C., JARVIS, I., HYDES, D.J., COLLEY, S. & WILSON, T.R.S. 1986 The behaviour of manganese in Atlantic carbonate sediments. Geochimica et Cosmochimica Acta, 50, 1807-1818.

8. WILSON, T.R.S. 1986 Vertical porewater advection investigated by means of a general diagenetic model. Science of the Total Environment, 49, 163-173.

9. FRANCIS, T.J.G., SEARLE, R.C. & WILSON, T.R.S. 1986 The oceanic sediment barrier. Philosophical Transactions of the Royal Society of London, A, 319, 115-137.

10. WILSON, T.R.S. & MILES, D.L. 1987 On the utility of chemical data for the detection of vertical pore-water movement in marine sediments. Initial Reports of the Deep Sea Drilling Project, 94, 1145-1148.

11. THOMSON, J., COLLEY, S., HIGGS, N.C., HYDES, D.J., WILSON, T.R.S. & SØRENSEN, J. 1987 Geochemical oxidation fronts in N.E. Atlantic distal turbidites and their effects in the sedimentary record. In, Geology and geochemistry of abyssal plains, (ed. P.P.E. Weaver and J. Thomson). Oxford: Blackwells for Geological Society. (Special Publication 31). (in press)

12. JARVIS, I. & HIGGS, N.C. 1987 Trace-element mobility during early diagenesis in distal turbidites: late Quaternary of the Madeira Abyssal Plain, N. Atlantic. In, Geology and geochemistry of abyssal plains, (ed. P.P.E. Weaver and J. Thomson). Oxford: Blackwells for Geological Society. (Special Publication 31). (in press)

13. SØRENSEN, J., JØRGENSEN, K.S., COLLEY, S., HYDES, D.J., THOMSON, J. & WILSON, T.R.S. 1987 Depth localisation of denitrification in a deep sea sediment from the Madeira Abyssal Plain. Limnology and Oceanography. (in press)

14. COLLEY, S. 1987 Uranium distribution in distal turbidites emplaced in pelagic conditions in the Great Meteor East area, Madeira Abyssal Plain. In, Geoscience investigations of two North Atlantic abyssal plains - the ESOPE international expedition, (ed. R.T.E. Schuttenhelm et al). Ispra: Joint Research Centre. (in press)

15. HYDES, D.J. 1987 Trace metals in solution at GME. Wormley: Institute of Oceanographic Sciences, 7pp. (Unpublished manuscript).

DEPARTMENT OF THE ENVIRONMENT
RADIOACTIVE WASTE MANAGEMENT
RESEARCH PROGRAMME 1979-1987

DoE Report No.:

Contract Title: Department of the Environment Marine Research Programme - Site Characterisation Studies

DoE Reference: PECD 7/9/308

Report Title: Geochemical Aspects - Final Report

Authors: J. Thomson, T.R.S. Wilson, S. Colley, N.C. Higgs, and D.J. Hydes

Date of submission to DoE:

ABSTRACT

This report summarises geochemical research carried out by the Institute of Oceanographic Sciences in connection with the DoE radioactive waste management research programme. It covers the period 1 April 1979 to 31 March 1987. Particular attention has been given to the "Great Meteor East" area of the Madeira Abyssal Plain, and to those natural geochemical species which show mobility in the sediment column.

Much of the work mentioned here is reported upon, usually in much greater detail, in a series of individual reports included here as Appendices.

Keywords: 299 DoE sponsored research
15 Heat generating
93 Disposal on deep ocean bed
94 Disposal under deep ocean bed

This work has been commissioned by the Department of the Environment as part of its radioactive waste management research programme. The results will be used in the formulation of Government policy but, at this stage, they do not necessarily represent Government policy.